NASA
Technical
Paper
3022

July 1990

Flight Characteristics of a Modified Schweizer SGS 1-36 Sailplane at Low and Very High Angles of Attack

Alex G. Sim

NASA

NASA Technical Paper 3022

1990

Flight Characteristics of a Modified Schweizer SGS 1-36 Sailplane at Low and Very High Angles of Attack

Alex G. Sim
Ames Research Center
Dryden Flight Research Facility
Edwards, California

National Aeronautics and Space Administration
Office of Management
Scientific and Technical Information Division

CONTENTS

SUMMARY

A manned flight research program using a modified sailplane was conducted to very high angles of attack at the NASA Ames Research Center's Dryden Flight Research Facility. Piloting techniques were established that enabled the pilot to attain and stabilize on an angle of attack in the 30° to 72° range. Aerodynamic derivatives were estimated from the flight data for both low and very high angles of attack and are compared to wind-tunnel data. In addition, limited performance and trim data are presented.

NOMENCLATURE

All the flight and predicted data are in body axis with X forward, Y to the right, and Z down. Unless otherwise noted, the results are presented at a center of gravity (c.g.) of 0.338 $\bar{c}$. Flight c.g. was either at 0.284 $\bar{c}$ or 0.338 $\bar{c}$.

a_n	acceleration in the minus body-Z direction, g
a_x	acceleration in the body-X direction, g
a_y	acceleration in the body-Y direction, g
b	reference span
$\bar{c}$	reference chord
c.g.	center of gravity
KEAS	equivalent airspeed, kn
L/D	lift-to-drag ratio
p	roll rate, deg/sec
$\dot{p}$	roll angular acceleration, deg/sec^2
pEst	parameter estimation (program)
q	pitch rate, deg/sec
$\dot{q}$	pitch angular acceleration, deg/sec^2
$\bar{q}$	dynamic pressure, lb/ft^2
R_N	Reynolds number
r	yaw rate, deg/sec
$\dot{r}$	yaw rate acceleration, deg/sec^2
TED	trailing edge down
TEL	trailing edge left
TEU	trailing edge up
v	true velocity, ft/sec
α	angle of attack, deg
β	angle of sideslip, deg
δ_a	aileron position, left–right, right TEU +, deg
δ_e	elevator position, TED +, deg
δ_r	rudder position, TEL +, deg
δ_{Stab}	stabilator position, TEU +, deg
θ	pitch angle, deg
ϕ	bank angle, deg

Coefficients

C_A	axial force
C_D	drag
C_ℓ	rolling moment
C_L	lift
C_m	pitching moment
C_n	yawing moment
C_N	normal force
C_Y	sideforce

Derivatives

C_{A_α}	partial derivative of C_A due to α, per deg
$C_{A_{\delta_e}}$	partial derivative of C_A due to δ_e, per deg
C_{ℓ_p}	partial derivative of C_ℓ due to $pb/2v$, per rad
C_{ℓ_r}	partial derivative of C_ℓ due to $rb/2v$, per rad
C_{ℓ_β}	partial derivative of C_ℓ due to β, per deg
$C_{\ell_{\delta_a}}$	partial derivative of C_ℓ due to δ_a, per deg
$C_{\ell_{\delta_r}}$	partial derivative of C_ℓ due to δ_r, per deg
C_{m_q}	partial derivative of C_m due to $q\bar{c}/2v$, per rad
C_{m_α}	partial derivative of C_m due to α, per deg
$C_{m_{\delta_e}}$	partial derivative of C_m due to δ_e, per deg
C_{n_p}	partial derivative of C_n due to $pb/2v$, per rad
C_{n_r}	partial derivative of C_n due to $rb/2v$, per rad
C_{n_β}	partial derivative of C_n due to β, per deg
$C_{n_{\delta_a}}$	partial derivative of C_n due to δ_a, per deg
$C_{n_{\delta_r}}$	partial derivative of C_n due to δ_r, per deg
C_{N_α}	partial derivative of C_N due to α, per deg
$C_{N_{\delta_e}}$	partial derivative of C_N due to δ_e, per deg

C_{Y_β} partial derivative of C_Y due to β, per deg

$C_{Y_{\delta_a}}$ partial derivative of C_Y due to δ_a, per deg

$C_{Y_{\delta_r}}$ partial derivative of C_Y due to δ_r, per deg

INTRODUCTION

Flight at very high angles of attack has occurred throughout aviation history. The 1902 Wright glider had a poststall "parachute" mode that was used as an emergency landing technique (ref. 1). Model airplanes have used a stabilator "dethermalizer" since the thirties (ref. 2) as a way of inducing a stabilized "deep stall" mode to landing. In recent years, the Kasperwing Ultralight (Cascade Ultralites Inc., Arlington, Washington) (ref. 3) has demonstrated a "vortex mush" flight mode. Common to these concepts are: (1) the stable descent with the main wing mostly stalled (that is, the airflow separated from the upper surface), and (2) poststall aerodynamics dominated by high-aspect-ratio wings rather than long forebodies or strakes. Pitch trim and control is achieved by maintaining attached flow on a secondary wing (horizontal stabilizer or canard). Other possible means of providing control include thrust modulation or vectoring, or vortex positioning using variable strakes or blowing. Possible future applications of this very high-angle-of-attack mode include: (1) emergency recoveries from spins or spiral dives, (2) near-vertical descents in areas of restricted lateral maneuvering, (3) safe recoveries of long-winged, high-altitude remotely piloted vehicle (RPV) aircraft, and (4) precision landings when used in conjunction with a retrorocket landing system.

There were two specific objectives of the high-angle-of-attack program conducted at NASA Ames Research Center's Dryden Flight Research Facility. The first objective was to demonstrate the feasibility of manned, controlled flight at very high angles of attack. This included refining the piloting techniques needed to safely make transition into, maneuver in, and recover from controlled flight at very high angles of attack. The second objective was to document the flight-determined aerodynamics and compare these data with available predictions.

During September and October 1983, 20 flights were conducted into the very high-angle-of-attack flight regime using a modified Schweizer SGS 1-36 sailplane (fig. 1). The SGS 1-36 sailplane was chosen because it is a low-speed vehicle, and its high-angle-of-attack aerodynamics are dominated by long wings rather than a long, pointed nose or forward strake. Aerodynamic characteristics were obtained in the 30° to 72° angle-of-attack range. Of particular interest were the stability and control derivatives, the trim data, and the piloting techniques required to safely enter and exit the very high-angle-of-attack flight regime. In 1984 a summary of these data was published in reference 4. However, less than half of the flight data at high angles of attack could be analyzed using the parameter estimation analysis tools that were available at that time. Recent advancements in these parameter estimation tools (ref. 5) have made possible a much more complete analysis of the data. This report presents the latest flight-determined aerodynamics that were obtained at both high (poststall) and low (normal) angles of attack.

TEST AIRCRAFT

The SGS 1-36 sailplane is a single-seat, T-tail design that is used commercially as an advanced trainer (fig. 2(a) and table 1). It is fabricated primarily of aluminum which allowed for easy modification of the horizontal tail, longitudinal control system, and cockpit area. To provide for adequate longitudinal control authority, the entire horizontal tail was modified to allow movement from 0° to 70° trailing-edge-up position (fig. 2(b)). A large lever located on the left side of the cockpit was used to position the horizontal tail (stabilator). The maximum stabilator position was adjusted between flights by the use of mechanical stops that corresponded to stabilator positions of 30°, 40°, 50°, and 60°. Elasticity in the stabilator's push-pull linkage allowed for approximately 3° of stabilator deflection because of airloads. The modifications to the horizontal tail and the associated control linkage additions required modifications to the vertical tail structure. The elevator, rudder, and aileron remained relatively unchanged. The cockpit area was significantly modified to enhance pilot egress. Other changes included: (1) a large, cranked noseboom (cranked to avoid the tow rope), (2) a cable brace extending from the forward turtle deck to the tip of the vertical tail, and (3) mass balance weights attached to short booms on the front of the stabilator.

The instrumentation consisted of 26 channels and was used for both aerodynamic analysis and to insure flight safety. The primary instrumentation system con-

sisted of linear accelerometer and rate gyro triads, a vertical gyro for roll and pitch attitude, airdata sensors, signal conditioning, a 10-bit pulse code modulation system, and a downlink transmitter. Most of the hardware was located on a removable pallet behind the pilot's seat. The airdata measurements were obtained using a self-aligning pitot-static head (fig. 2(c)). The angle-of-attack and angle-of-sideslip vanes were located on the noseboom aft of the self-aligning airdata head. Direct measurements were made of elevator, stabilator, and rudder position. The left-aileron position was indirectly measured from the push-tube linkage near the wing root. Total aileron position was computed postflight from the left-aileron position. The measured data were transmitted to a ground facility for real-time monitoring and recording.

As a result of the vehicle modifications, instrumentation system, and additional ballast to offset the modifications, the vehicle was flown at weights from 874 to 900 lb. Since the gross weight limit for the baseline SGS 1-36 sailplane is 710 lb, maneuver limit load factor for the modified vehicle was reduced from 5.33 to 3.89 g. Another precaution was to reduce maximum airspeed from 123 to 97 mi/h. The configuration was shown to be free of flutter to an airspeed of 97 mi/h using a ground test vehicle (ref. 6).

The moments of inertia (table 2) were determined experimentally using a conventional moment of inertia swing similar to that described in reference 7. The vehicle was flown at a center of gravity (c.g.) of 33.8 percent for flights 1 to 8, and a c.g. of 28.4 percent for flights 9 to 20.

PREFLIGHT PREPARATIONS

A limited wind-tunnel test was conducted in the NASA Langley 30- by 60-Foot Wind Tunnel using a 1/4-scale model (ref. 8). Force and moment data were obtained and used to generate an aerodynamic model that constituted the best preflight set of predictions for the static derivatives. To limit the scope of the test, a coarse grid of angles of attack and sideslip was used. The grid was especially coarse at low angles of attack. To limit model loading, testing was done at a low dynamic pressure. The resulting wind-tunnel Reynolds number was 180,000, based on mean wing chord. The flight vehicle operated at approximately 10 times this Reynolds number. Data from other studies (fig. 3 and ref. 8) have shown that representative trends can be obtained from model tests at low Reynolds numbers for data at angles of attack outside of the poststall transition area. However, within the transition area the low Reynolds number data are not a good representation of the higher Reynolds number data. Thus, the SGS 1-36 wind-tunnel data in the 5° to 30° angle-of-attack range should be treated with caution. Also, inconsistencies with low Reynolds number testing are especially prevalent when predicting trailing-edge control surface effects. The wind-tunnel data are considered to be the minimum necessary to conduct the flight program safely and are representative of the level of results that can be obtained from small-scale, free-flight models, drop models, or spin tests. The damping parameters used for the aerodynamic model and the preflight predicted data set were obtained using a combination of calculated methods, including those in reference 9.

Prior to conducting the manned flight tests, many unmanned tests were conducted using radio-controlled models of similar geometries. These tests provided insight into the physics of the maneuver and yielded a technique for the entry and recovery from high-angle-of-attack flight without encountering a spin. When the models were intentionally put into a spin, spin recovery was attained faster by deep stalling to very high angle of attack and then recovering than by using conventional spin recovery techniques.

In addition, prior to the manned flight tests, the aerodynamic model was implemented in a manned, real-time simulation, similar to those discussed in reference 10. The simulator was used to refine the high-angle-of-attack flight technique and for flight planning. The simulator consisted of a fixed-based cockpit utilizing an eight ball for attitude reference and dial instruments for angles of attack and sideslip, normal acceleration, and control surface positions.

PILOTING TECHNIQUE RESULTS

The concept of high-angle-of-attack flight is illustrated in figure 4. At high angles of attack, a condition exists where the wing is fully stalled while the tail is attached and somewhat aligned with the airstream. An example of a high-angle-of-attack maneuver in figure 5 shows the entry into stalled flight, the flight at high angle of attack, and the recovery. On a typical test flight, the vehicle was towed to 8500 ft above ground level and released. The vehicle was then decelerated to near-

stall airspeed using the elevator control (not shown). The technique used to enter high-angle-of-attack flight was to firmly position and then manually hold the stabilator at the ground-adjustable stop. The total time required to position the stabilator and achieve controlled deep stall was approximately 2 sec. The elevator was then used for maneuvering and minor trim changes. It was necessary to enter high-angle-of-attack flight rapidly to avoid lingering in the transition area where the airplane was susceptible to spins. The transition area (fig. 6) is characterized by large asymmetries in the lateral-directional forces and moments that are coupled with an aerodynamic unsteadiness. On the test vehicle, it was not possible to stabilize in the transition area even though significant control effectiveness was available.

After the rapid but smooth transition to high-angle-of-attack flight, the vehicle would quickly stabilize with a near-zero pitch attitude. The angle of attack would settle between 30° and 72°, depending on stabilator, elevator, and c.g. positions. Descent rate would be approximately 4000 ft/min. Approximately 1 min of data was obtained before the recovery altitude was reached (5000 ft above ground level). During this time, a trim point was attained followed by elevator, rudder, and aileron doublets. The doublets were used for postflight parameter estimation analysis. The pilot would then perform maneuvers to assess vehicle handling qualities.

The handling qualities evaluations concentrated on the basic flying tasks. During the stabilized portions of high-angle-of-attack flight, maneuvers were performed to investigate the handling qualities and included the ability to: (1) maintain steady flight, (2) change trim, and (3) change heading. The longitudinal handling qualities were generally acceptable to attain the desired angle of attack. The lateral-directional handling was often degraded by the presence of a slow oscillation (wing rock), particularly at the very high angles of attack. Lateral-directional handling qualities were further degraded by unstable hinge moments for both aileron and rudder. For the last few flights, the ailerons were sealed using a lower surface fairing. The seal brought the aileron hinge moment back to neutral and improved the handling qualities.

Recovery was initiated by using the stabilator to decrease the angle of attack to near the transition area (between 25° and 30°). Although the actual angle of attack was not displayed in the cockpit, the transition area was sensed by the pilot from both the tail buffet (because of wing wake) and the aerodynamic unsteadiness. The stabilator was then rapidly moved to the zero or baseline position. During recovery, 300 to 500 ft of altitude were used while the airspeed typically increased from 38 to 55 kn. Recovery was very docile when accomplished in this manner.

FLIGHT DATA ANALYSIS

Flight Data

Because of buffet at high angles of attack the separated flow over the wing and fuselage induced a significant amount of vibration into the vehicle structure. This induced a high-frequency component on to the measured flight data. For the analysis in this report, this high-frequency component was effectively noise on the data. The buffet was always present at high angle of attack but worse in the 27° to 35° angle-of-attack range where the wing wake washed over the stabilator. The low speed and low wing loading made the vehicle susceptible to even very light levels of atmospheric turbulence. Since turbulence is not a modeled input for the estimation analysis, it is avoided where possible. However, the limited number of maneuvers (especially at high angle of attack) and short flight times necessitated using maneuvers with very light turbulence. Light turbulence and the effective noise tend to make the data analysis less certain and thus yield more scatter in the results.

Corrections, similar to those in reference 11, were applied to the flight measurements to correct the sensors for slight axis misorientation, and to shift them to the vehicle flight c.g. Even with many corrections and postflight analyses, the angles of attack and sideslip were not precise measurements. It is suspected that the vanes were adversely influenced by the noseboom presence (especially at the high angles of attack), noseboom vibration, and the wake from the relatively large pitot-static head (fig. 2(c)). The low-angle-of-attack data (potential flow) were corrected for upwash using simple slope and bias as shown in equation (1).

$$\alpha_{corrected} = \alpha_{indicated} \times (0.88) - 0.72 \quad (1)$$

This linear upwash correction was obtained using a potential flow-field solution (ref. 9). Upwash corrections

using potential flow theory were not considered valid at very high angles of attack. An examination of photographs of yarn streamers at 60° angle of attack did confirm the indicated angles to be approximately correct. Another attempt to check on the validity of angle of attack at high angles was conducted during an earlier parameter estimation analysis of these same flight data. A parameter equivalent to the slope term in equation (1) was estimated and yielded a value generally near unity but with substantial scatter. The angular accelerations were computed postflight from the angular rates using the least squares slope of a 5-point sliding window at 50 samples/sec.

Estimation Process

A parameter estimation analysis of the flight data was performed using version 2.2 of pEst, a parameter estimation program (which is similar to the version in ref. 5). The pEst program is an interactive, nonlinear program for the analysis of dynamic systems. This analysis used the standard pEst user routines that define the aircraft six-degree-of-freedom nonlinear set of differential equations. Although full coupling of the equations was investigated, it was found to be undesirable since the maneuvers were performed in a decoupled manner. Thus, the aerodynamic part of the equations were split into either longitudinal- or lateral-directional subsets, while the inertial part of the equations maintained their full nonlinearity. Nonlinearities in aerodynamic parts of the equations (derivatives) were also investigated but ultimately not used. The relatively small number of maneuvers available for analysis, coupled with the high levels of noise on the measured flight data, precluded a more extensive modeling study. The variables $\bar{q}$, v, α, β, θ, and ϕ varied with time throughout the maneuvers. The results of the pEst analysis were sets of lateral-directional or longitudinal stability and control derivatives. These flight-determined derivatives were used to refine the predicted aerodynamic model at low and very high angles of attack.

Although angles of attack, pitch, sideslip, and roll were used as active states (in their respective lateral-directional or longitudinal subsets), their corresponding responses were relatively lightly weighted. For example, there was only a slight penalty in the analysis for poorly matching (fitting) the measured and computed angle of attack. The results of prior pEst and other maximum likelihood analyses (ref. 4) were used as starting values and *a priori* reference values. A low weighting was placed on these values to lessen the scatter in the final results. Care was taken to limit the *a priori*'s cost function to approximately one percent of the total cost. During the lateral-directional high-angle-of-attack analysis, it was necessary to manually adjust the aileron derivatives until a good match was attained between the computed and measured acceleration responses during the aileron input. For example, the value of the change in sideforce due to aileron derivative was often manually adjusted until the computed and measured time history of lateral acceleration matched during the aileron control input. Occasionally, it was necessary to manually adjust the rudder derivatives in a similar fashion. Derivatives that have been manually adjusted are shown on the plots without the uncertainty bounds.

AERODYNAMIC RESULTS

Trim

The longitudinal trim envelopes (fig. 7) are presented for a family of stabilator settings at the two flight c.g. locations. Note that for the high-angle-of-attack data, the average stabilator settings were approximately 3° lower than their commanded position because of control linkage flexure. From the trim envelopes, it was evident that control authority was available to attain stabilized flight over the desired angle-of-attack range, and the vehicle had stable static longitudinal stability at both flight c.g. locations. A conventional plot of the trim data at low angle of attack (fig. 8) shows an increasing longitudinal stability with angle of attack and, as expected, with forward c.g. location.

Performance

The traditional aerodynamic efficiency factor, lift-to-drag ratio (L/D), for the baseline and modified SGS 1-36 sailplane is presented in figure 9 as a function of equivalent velocity. The baseline data (ref. 12) are presented with an adjusted velocity to normalize both sets of data to the same gross weight. For the modified vehicle, data were generated using the accelerometer analysis technique (ref. 13). As expected, the modified SGS 1-36 sailplane had lower aerodynamic performance because of its extensive

modifications, however, performance was acceptable to conduct the flight tests. In high-angle-of-attack flight, aerodynamic performance was low and airspeed changed only slightly with angle of attack. A better indicator of the performance at high angle of attack is the sink rate. The sink rate for the modified SGS 1-36 sailplane is shown in figure 10 as a function of the horizontal component of velocity. The sink rates in the high-angle-of-attack region were as high as 4200 ft/min.

Longitudinal Derivatives

Insight into the general nature of the longitudinal characteristics can be gained by looking at maneuver time histories at both low and high angles of attack. The low-angle-of-attack maneuver (fig. 11) shows: (1) the measured data were free of significant noise, (2) the transient response to the elevator doublet was highly damped, and (3) except for angle of attack, the fit between the measured and computed data was excellent. Because of the high damping, the low-angle-of-attack maneuvers were often expanded to include two elevator doublets separated by 3 to 5 sec of no control input. The high-angle-of-attack maneuver example (fig. 12) contrasts with the low-angle-of-attack maneuver by having: (1) noise on the rates and accelerations data, (2) a response that appears lightly damped, and (3) not as good a fit of the measured and computed data. The noise on the data at high angles of attack led to scatter and higher uncertainty bounds. The inability to accurately fit the measured data suggests the probability of a modeling error.

The longitudinal derivatives in figures 13(a) through 13(g) present the flight results, a recommended fairing of the flight data, and the predicted data set. Note that the terms "predicted data" or "predictions" refer to static derivatives derived from wind-tunnel sources and dynamic derivatives derived from engineering calculations. The change in the derivative of axial force coefficient due to angle of attack, C_{A_α} (fig. 13(a)), was in good agreement with predictions at angles of attack below 2° and in fair agreement at higher angles of attack. The discrepancy in the 5° to 10° angle-of-attack range was considered to be a result of the large Reynolds number discrepancy between wind-tunnel and flight tests as previously discussed and shown in the example data of figure 3. Note, for a high-aspect-ratio configuration like the SGS 1-36 sailplane, the axial force is dominated by the lift effects at angles of attack greater than 5° (that is, 11° angle of attack above zero lift).

The static longitudinal stability derivative, C_{m_α} (fig. 13(b)), shows very low stability values for the $-3°$ to 0° angle-of-attack range. By 10° angle of attack, the stability derivative was reasonably high. This change in static stability at the lower angles of attack was consistent with the trim data of figure 8. At the higher angles of attack, the flight derivatives were scattered due to the noise on the data (fig. 12). The noise tended to mask the short-period frequency transient information from which the flight derivatives are determined.

The normal-force derivative, C_{N_α} (fig. 13(c)), was generally higher than predicted in the high-angle-of-attack range. In the low-angle-of-attack range, both flight data and predictions had similar trends.

The elevator control derivatives (figs. 13(d) to 13(f)) show the vehicle to have higher than predicted control effectiveness at low and high angles of attack. The constant values shown for the predictions were a result of the inability to determine a consistent trend with angle of attack due to scatter in the wind-tunnel data.

The pitch damping derivative, C_{m_q} (fig. 13(g)), was lower than predicted at low angles of attack and somewhat indeterminate at high angles of attack. Due to noise on the measurements (fig. 12) a situation existed where stability and damping could be "traded" effectively within the pEst analysis. Some of the more apparent trades could be implied from the data near 10° and near 32° angle of attack when comparing C_{m_q} and C_{m_α} (fig. 13(b)).

Lateral-Directional Derivatives

A typical low-angle-of-attack, lateral-directional maneuver time history (fig. 14) shows: (1) the measured data exhibited only slight structural noise, (2) the transient response from both aileron and rudder had high damping, and (3) there was an excellent fit between the measured and the computed time histories. The aileron control input coupled into the directional axis, while the rudder input shows only slight lateral coupling. The fit between the measured and the computed angle of sideslip (not shown) was similar to the fit observed for angle of attack in figure 11. Sideslip angle was weighted low enough that it was essentially

not used so it was a very minor contributor to the pEst analysis. The high-angle-of-attack flight data of figure 15 shows an increase in noise over the low-angle-of-attack data of figure 14. However, the noise on the high-angle-of-attack data was not as severe as shown on the longitudinal flight data of figure 12. The damping was masked by the presence of both the low-level oscillations (wing rock) and the nearly continuous control input from either the aileron or rudder. There was a good fit between the measured and computed time histories, with the exception of roll rate and roll angular acceleration resulting from the last part of the aileron input. In this example, the estimate for $C_{\ell_{\delta_a}}$ was manually adjusted until the measured and computed time histories of the roll angular acceleration were a good fit during the initial part of the aileron input.

For the high-angle-of-attack data set, it was not possible to obtain a good fit of the lateral time response during all of the aileron doublet input. This indicates a probable error in the modeling of the ailerons using linearized parameters in the form of traditional partial derivatives. In an earlier pEst high-angle-of-attack analysis of these flight data, a piecewise linear model was used to represent suspected aileron nonlinearities by defining additional derivatives for large aileron deflections. This approach was abandoned when inconsistent aileron derivatives were obtained. The approach of the analysis for this report was to obtain the aileron derivatives that best describe the time response to the initial aileron doublet.

The sideslip derivatives are presented in figures 16(a) through 16(c). The effective dihedral derivative, C_{ℓ_β} (fig. 16(a)), shows that the flight data at low angles of attack had a similar trend, but at lower levels than predicted. The flight data at high angles of attack were well-defined but very different than predicted. During the wind-tunnel test, a configuration was tested with the wings constrained in bending (wire braced) but it yielded only minor changes in the C_{ℓ_β} predictions. The differences cannot be explained by wing bending of the wind-tunnel model. The directional or weathercock stability derivative, C_{n_β} (fig. 16(b)), shows reasonable correlation at low angle of attack and similar trends with values lower than predicted at the high angles of attack. Similarly, the sideforce derivative, C_{Y_β} (fig. 16(c)), had trends similar to the predictions but was less negative at both high and low angles of attack.

As previously discussed, most of the aileron derivatives (figs. 16(d) to 16(f)) were manually adjusted to their current values and are presented without their uncertainty bound. The primary roll control derivative, $C_{\ell_{\delta_a}}$ (fig. 16(d)), is shown to have a trend similar to the predictions but at a much lower value. The aileron was not very effective at the high angles of attack, however, sufficient control power was available to gently maneuver the airplane. The yaw due to aileron derivative, $C_{n_{\delta_a}}$ (fig. 16(e)), was generally near zero but was slightly proverse at low angles of attack and slightly adverse at high angles of attack. It was of an acceptably low value to yield good handling qualities and it was close to predictions. The derivative representing the sideforce generated by the aileron, $C_{Y_{\delta_a}}$ (fig. 6(f)), was also near zero and close to predictions and was thus consistent with $C_{n_{\delta_a}}$.

The roll due to rudder derivative, $C_{\ell_{\delta_r}}$ (fig. 16(g)), was slightly positive at the low angles of attack and near predictions, but near zero and close to predictions at the high angles of attack. The primary yaw control derivative, $C_{n_{\delta_r}}$ (fig. 16(h)), was significantly more effective (higher negative value) than predicted, especially at low angle of attack. The sideforce due to rudder derivative, $C_{Y_{\delta_r}}$ (fig. 16(i)), was also significantly higher than predicted and was consistent with $C_{n_{\delta_r}}$. Control with rudder was sufficient to gently maneuver the airplane at high angles of attack.

The damping derivatives (figs. 16(j) to 16(m)) were compared to calculated predictions. The primary roll damping derivative, C_{ℓ_p}, was lower than predicted but has consistent trends. At the higher angles of attack the damping derivatives represent both aerodynamic damping and any forcing functions such as asymmetric vortex shedding. With a forcing function it is physically possible for a primary damping derivative to have a positive (destabilizing) value as was the case with C_{ℓ_p} for angles of attack above 52°. The damping in yaw due to roll rate derivative, C_{n_p} (fig. 16(k)), shows low-angle-of-attack characteristics were well-defined and more negative than predicted. At high angles of attack, C_{n_p} was near zero. The damping in roll due to yaw rate derivative, C_{ℓ_r} (fig. 16(l)), was near predictions at low angle of attack but had excessive scatter and was poorly defined in the high-angle-of-attack range. The primary yaw damping derivative, C_{n_r} (fig. 16(m)), was generally lower than predicted at low angles of attack

and nearly indeterminate due to scatter at high angles of attack.

CONCLUDING REMARKS

The following conclusions can be drawn from the results of a manned, low-speed flight research program that was conducted to very high angles of attack.

1. Piloting techniques were established that allowed the pilot to safely make entry into, maneuver in, and recover from controlled flight within the 30° to 72° angle-of-attack range. Maneuvers performed to enter into and recover from deep stalled flight were docile. Stabilized flight at very high angles of attack yielded handling qualities that were acceptable to gently maneuver the airplane.

2. A maximum likelihood analysis technique was used to obtain aerodynamics derivatives from flight data at both low and very high angles of attack. These data were compared to the predicted data set and generally yielded fair-to-good agreement. The derivatives were also used to refine the aerodynamic database at low and very high angles of attack.

3. An analysis of the flight data was also used to better define the vehicle trim and the operational performance envelope. Control authority was available to trim the airplane in the 30° to 72° angle-of-attack range. At low angles of attack, performance remained acceptably high to conduct the flight research experiments. At the very high angles of attack, sink rates were approximately 4000 ft/min.

REFERENCES

1. Combs, Harry, *Kill Devil Hill*, Houghton Mifflin Co., 1979.

2. Goldberg, Carl, "Bring Them Down Safely," *Model Airplane News*, vol. 29, Sept. 1943, pp. 18–20.

3. Horne, Thomas A., "Redemption at Issaquah," *AOPA Pilot*, vol. 24, no. 5, 1981, pp. 57–60.

4. Sim, Alex G., *Flight Characteristics of a Manned, Low-Speed, Controlled Deep Stall Vehicle*, AIAA 84-2074, AIAA Atmospheric Flight Mechanics Conference, Seattle, Washington, Aug. 21–23, 1984. Also published as NASA TM-86041, 1984.

5. Murray, James E., and Richard E. Maine, *pEst Version 2.1 User's Manual*, NASA TM-88280, 1987.

6. Kehoe, Michael W., and Joseph F. Ellison, *Flutter Clearance of the Schweizer 1-36 Deep-Stall Sailplane*, NASA TM-85917, 1985.

7. Retelle, John P., Jr., *Measured Weight, Balance, and Moments of Inertia of the X-24A Lifting Body*, AFFTC-TD-71-6, 1971.

8. Paulson, John W., *Low Speed Wind Tunnel Investigation of a 0.25-Scale Model Similar to the Schweizer SGS 1-36 Sprite Sailplane*, Dynamic Engineering, Inc., Technical Report D-086, 1983.

9. Lamar, John E., and Blair Gloss, *Subsonic Aerodynamic Characteristics of Interacting Lifting Surfaces with Separated Flow Around Sharp Edges Predicted by a Vortex-Lattice Method*, NASA TN D-7921, 1975.

10. Smith, J.P., Lawrence J. Schilling, and Charles A. Wagner, *Simulation at the Dryden Flight Research Facility from 1957 to 1982*, NASA TM-101695, 1989.

11. Gainer, Thomas G., and Sherwood Hoffman, *Summary of Transformation Equations and Equations of Motion Used in Free-Flight and Wind-Tunnel Data Reduction and Analysis*, NASA SP-3070, 1972.

12. Johnson, Richard H., "Flight Test Evaluation of the Schweizer 1-36," *Soaring*, vol. 46, no. 3, Mar. 1982, pp. 36–38.

13. Beeler, De E., Donald R. Bellman, and Edwin J. Saltzman, *Flight Techniques for Determining Airplane Drag at High Mach Numbers*, NACA TN 3821, 1956.

Table 1. General data.

Fuselage:	
Overall length (less noseboom), ft	20.6
Wing:	
Area and reference area, ft^2	140.72
Span and reference span, ft	46.17
Reference chord, ft	3.28
Chord, root (centerline), ft	4.20
Chord, tip, ft	1.89
Incidence, root, deg	1
Incidence, tip, deg	0.065
Aileron area, ft^2	10.90
Airfoil section, root (to wing station 163)	FX 61-163
Airfoil section, tip	FX 60-126
Horizontal tail:	
Area, total, ft^2	13.15
Span, ft	7.92
Chord, root, ft	1.86
Chord, tip, ft	1.38
Incidence, TEU, deg	1.9
Elevator area, ft^2	4.48
Airfoil section	NACA 64_1-012
Vertical tail:	
Area, effective, ft^2	10.44
Span, effective, ft	4.33
Chord, effective, ft	2.41
Rudder area, ft^2	4.72
Airfoil section	NACA 64_1-012

Table 2. Mass properties.

	Flights 1 to 8	Flights 9 to 20
Center of gravity, $\bar{c}$	0.338	0.284
Gross weight, lb	874	900
Rolling moment of inertia, slug-ft^2	1014	1015
Pitching moment of inertia, slug-ft^2	641	672
Yawing moment of inertia, slug-ft^2	1633	1663
X–Z cross product of inertia, slug-ft^2	49.4	54.5

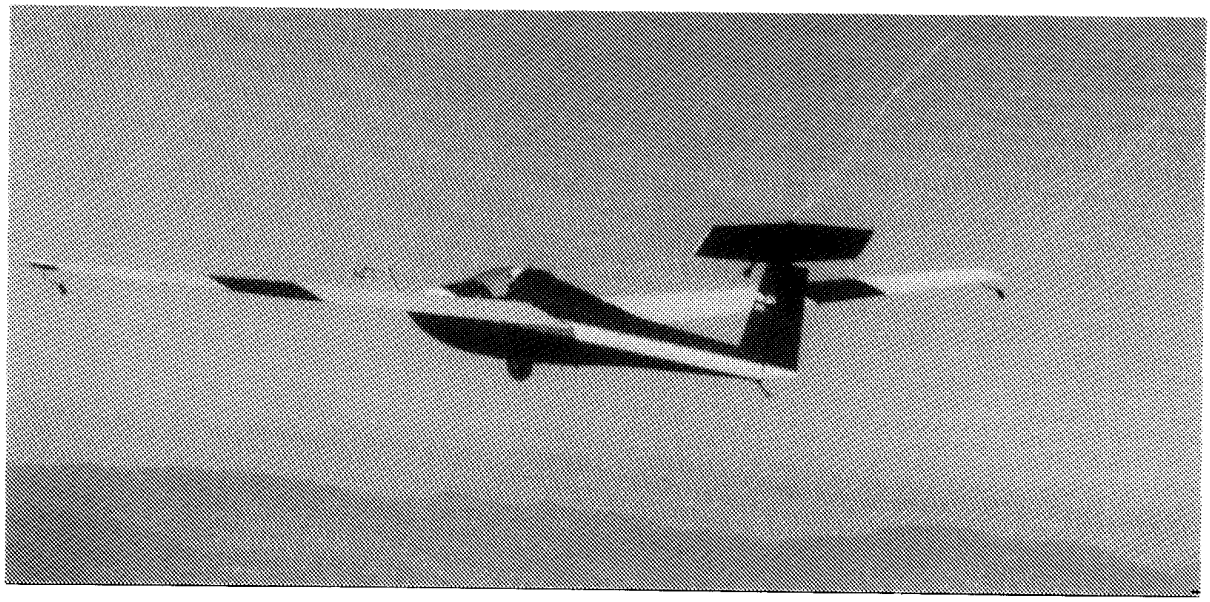

ECN 26846

Figure 1. Modified Schweizer SGS 1-36 sailplane at $\alpha = 50°$.

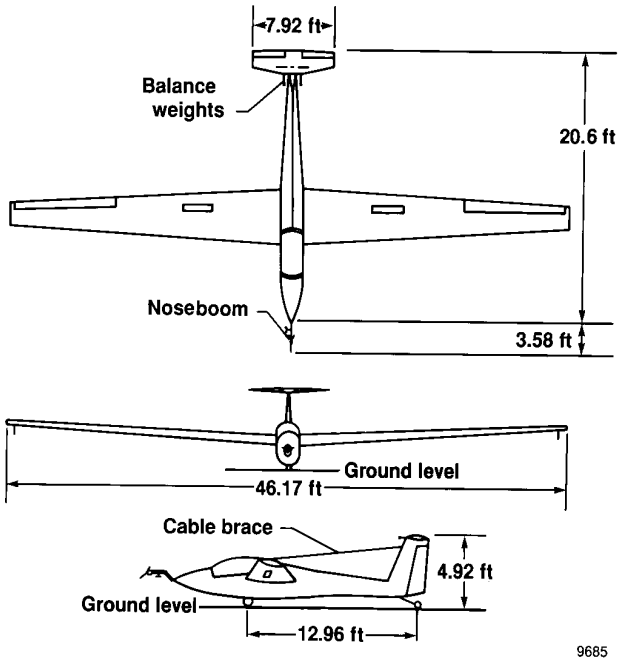

(a) Three-view drawing.

Figure 2. Modified SGS 1-36 sailplane.

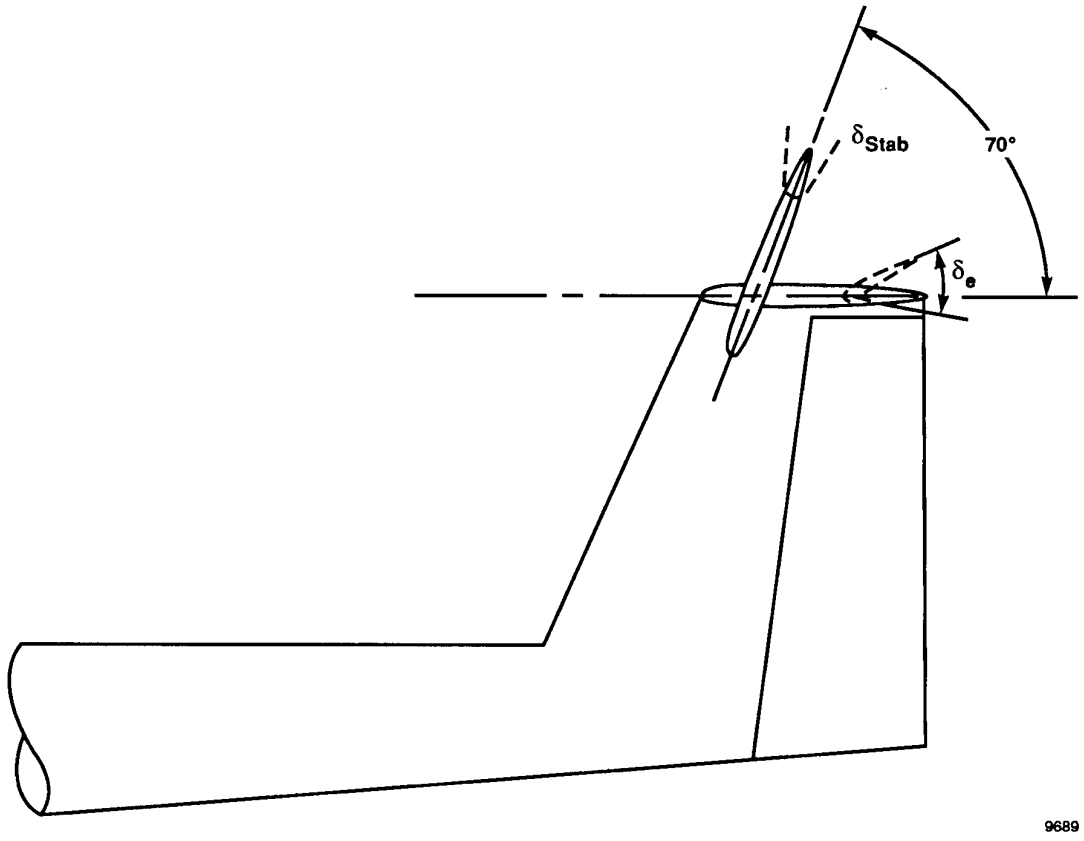

(b) Stabilator deflection at the 70° maximum position.

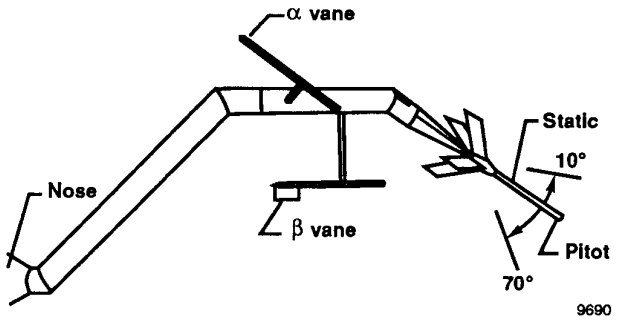

(c) Cranked noseboom with self-aligning pitot-static head.

Figure 2. Concluded.

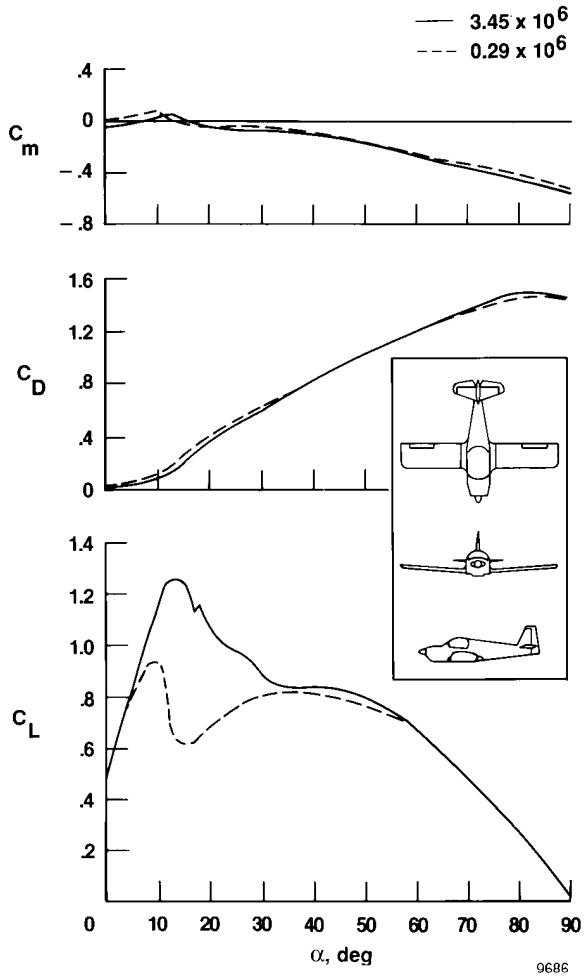

Figure 3. Effect of Reynolds number on longitudinal characteristics of a light plane.

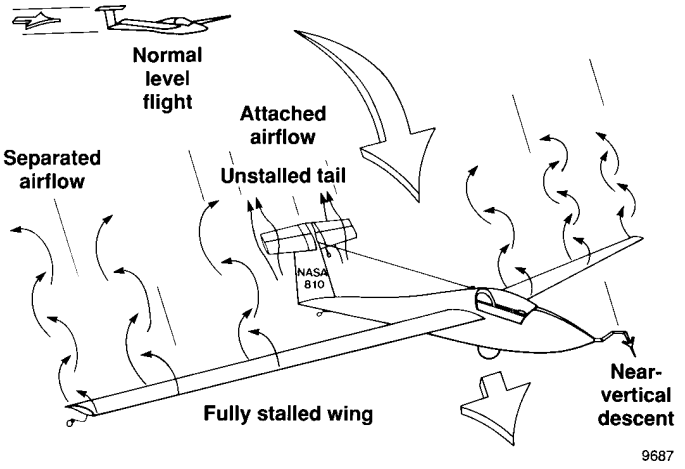

Figure 4. Basic concept of flight at very high angles of attack.

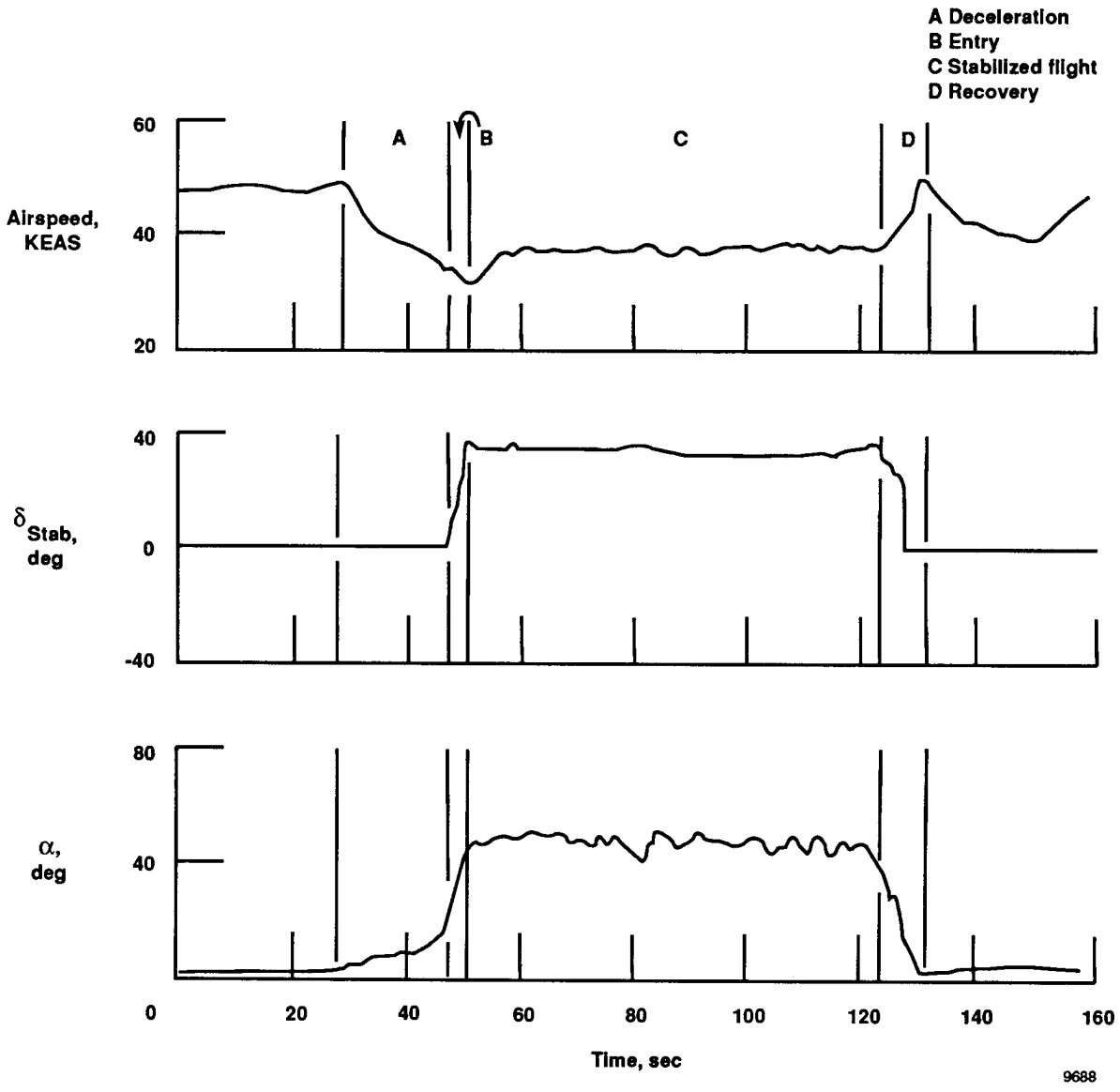

Figure 5. High-angle-of-attack flight maneuver.

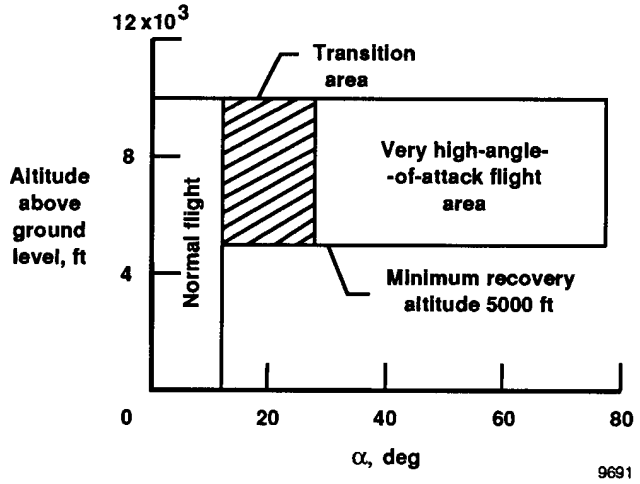

Figure 6. Operational flight envelope.

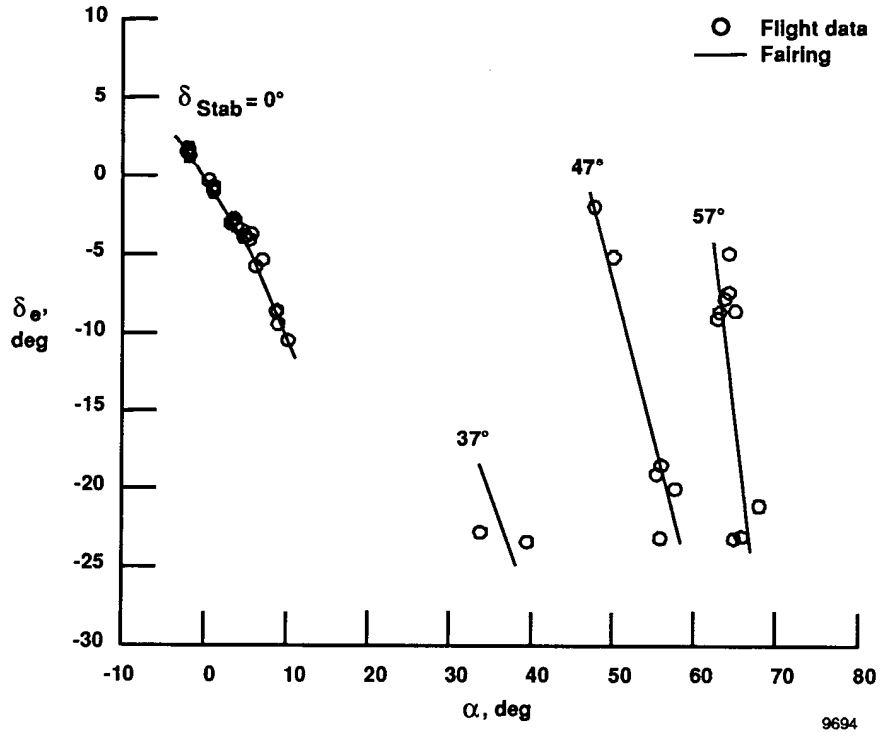

(a) c.g. = 0.284 $\bar{c}$.

Figure 7. Trim envelope for a family of stabilator settings.

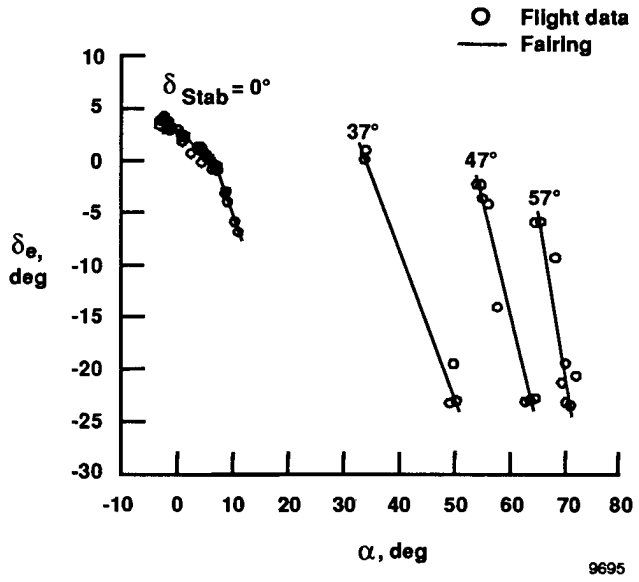

(b) c.g. = 0.338 $\bar{c}$.

Figure 7. Concluded.

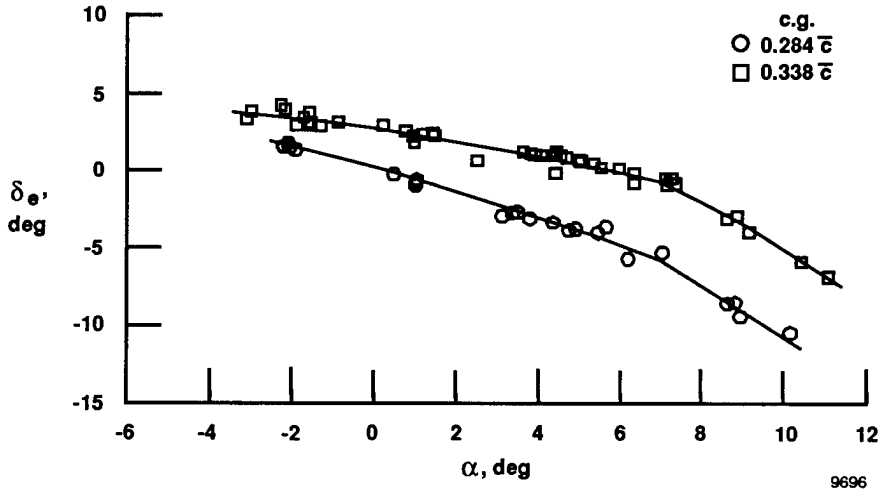

Figure 8. Trim curves for the zero stabilator setting.

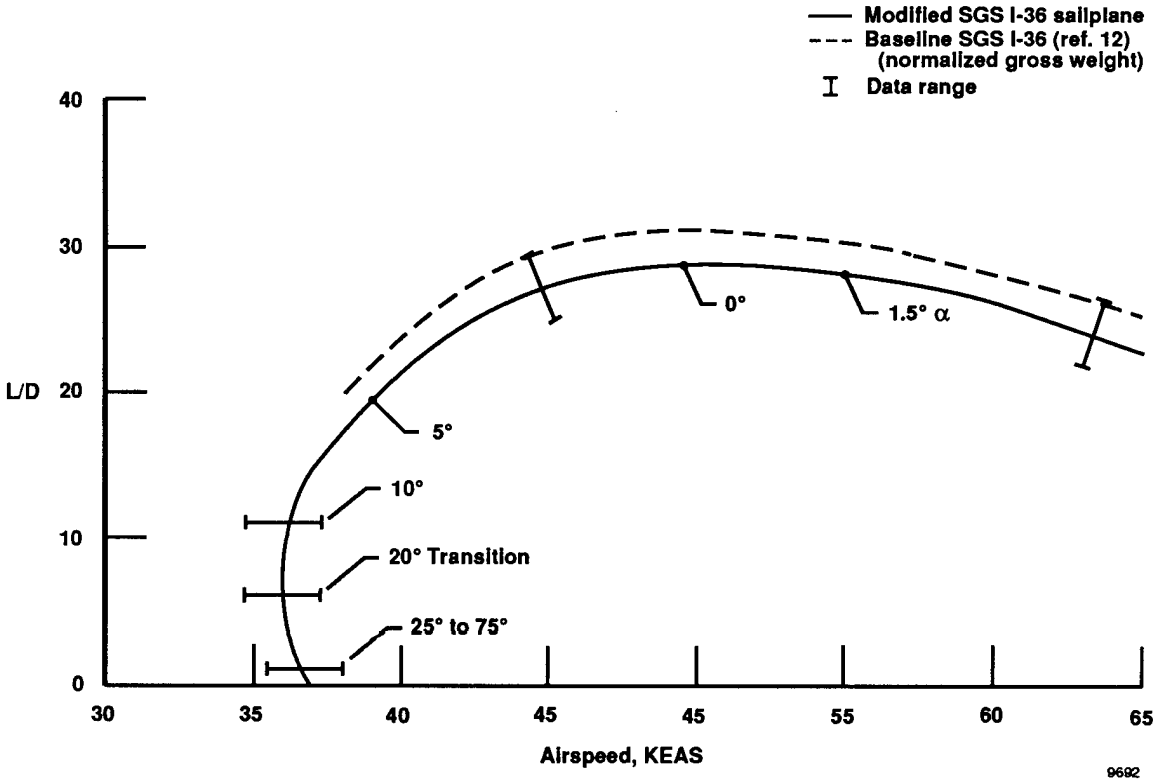

Figure 9. Flight data fairings of aerodynamic performance; gross weight = 873 lb.

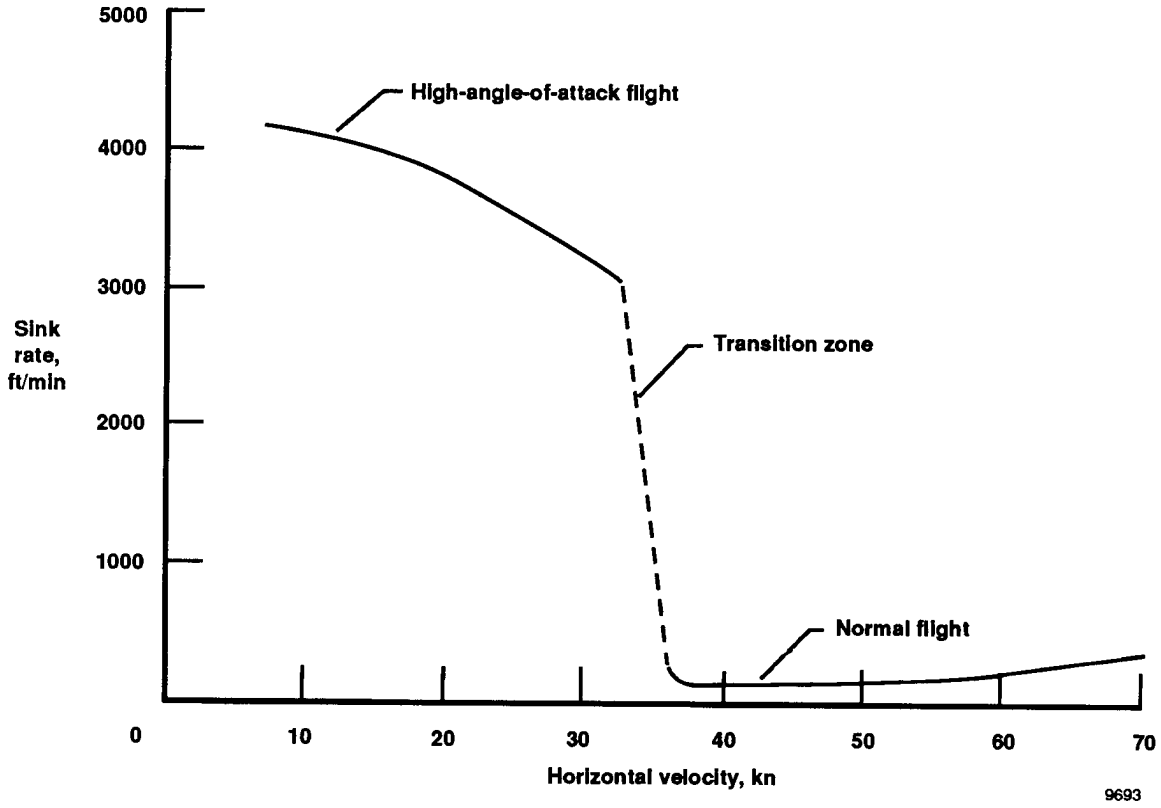

Figure 10. Flight data fairings of sink rate; gross weight = 873 lb.

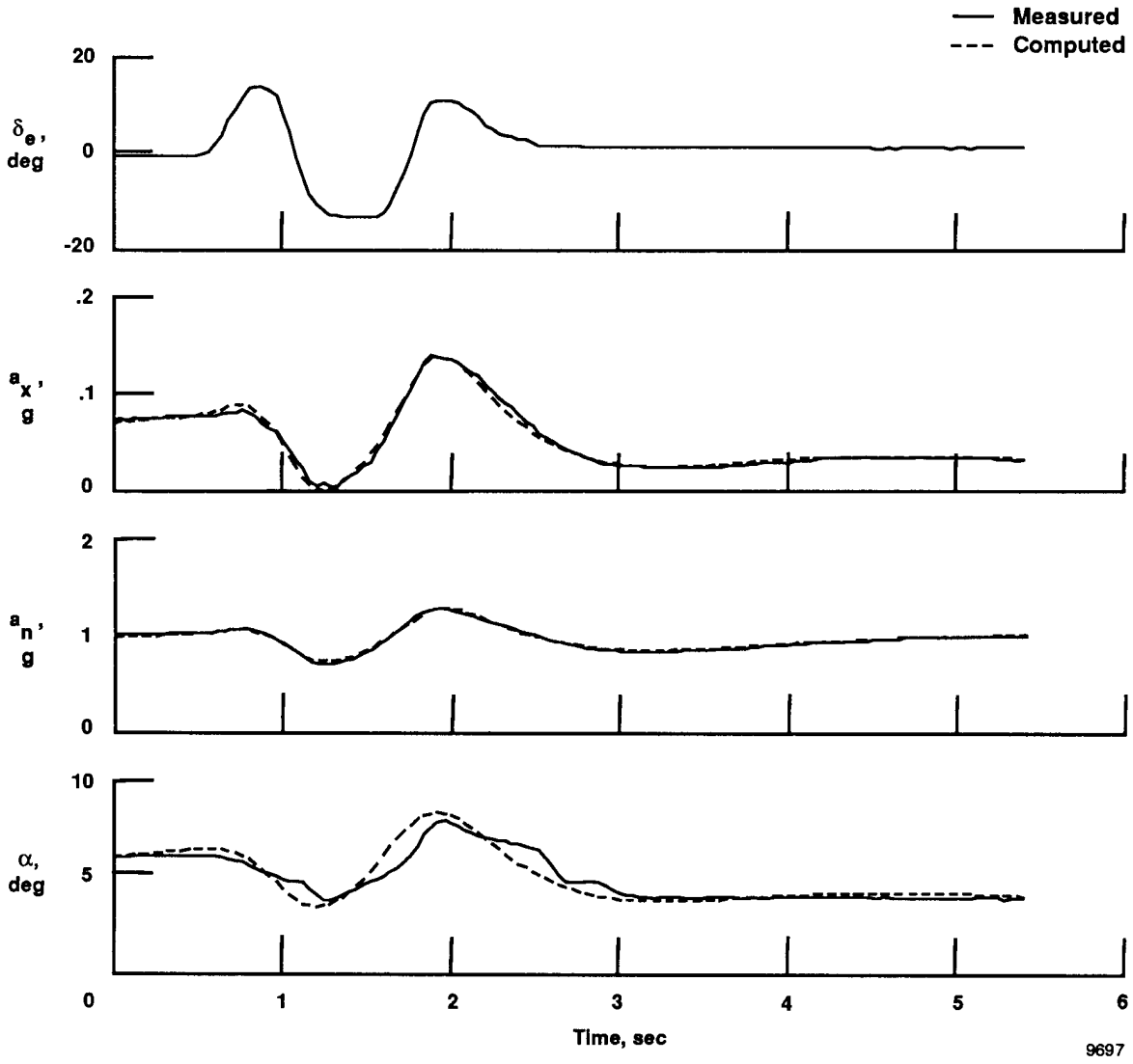

(a) Force axes.

Figure 11. Longitudinal maneuver at an average $\alpha = 5.0°$.

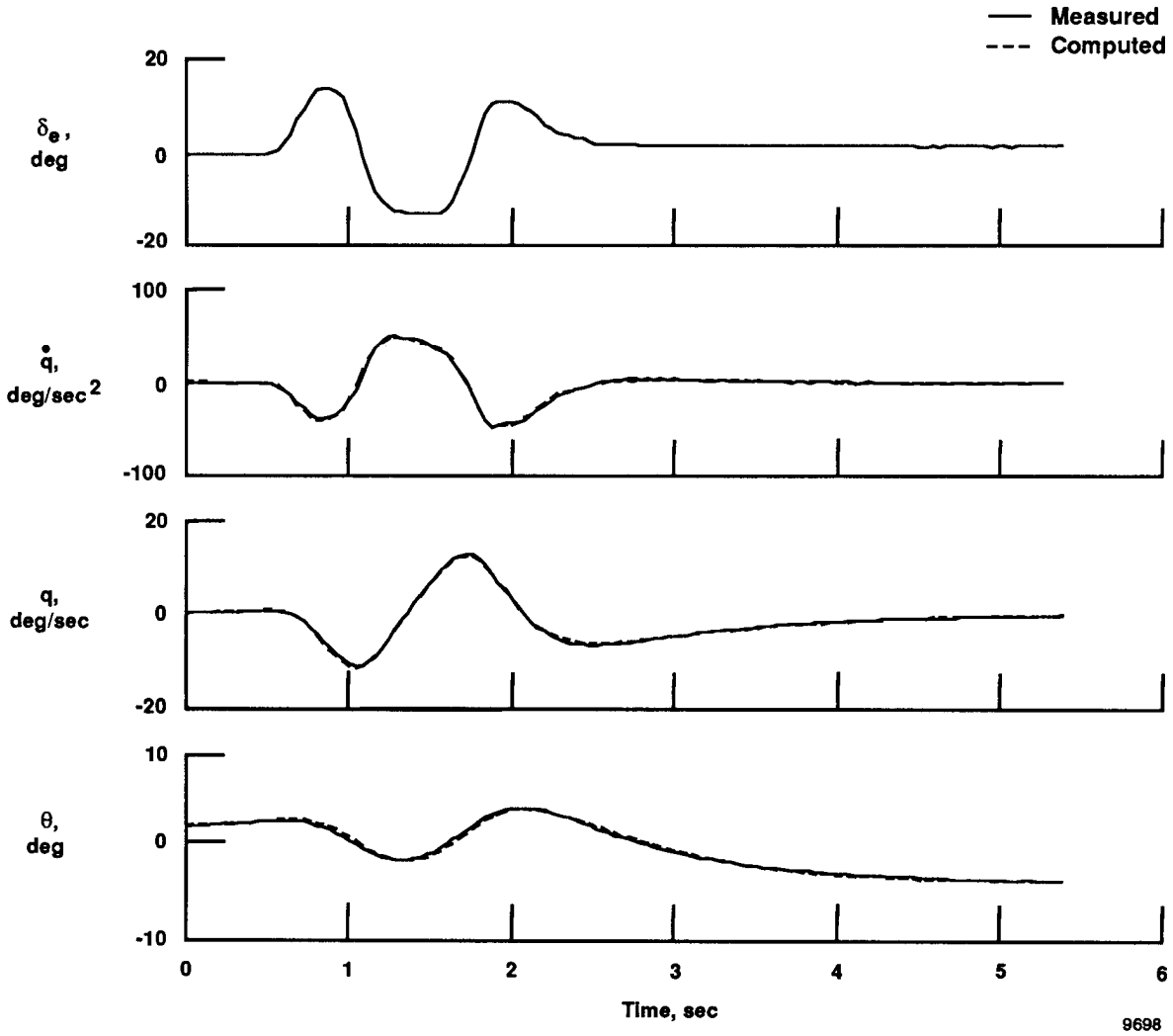

(b) Moment axis.

Figure 11. Concluded.

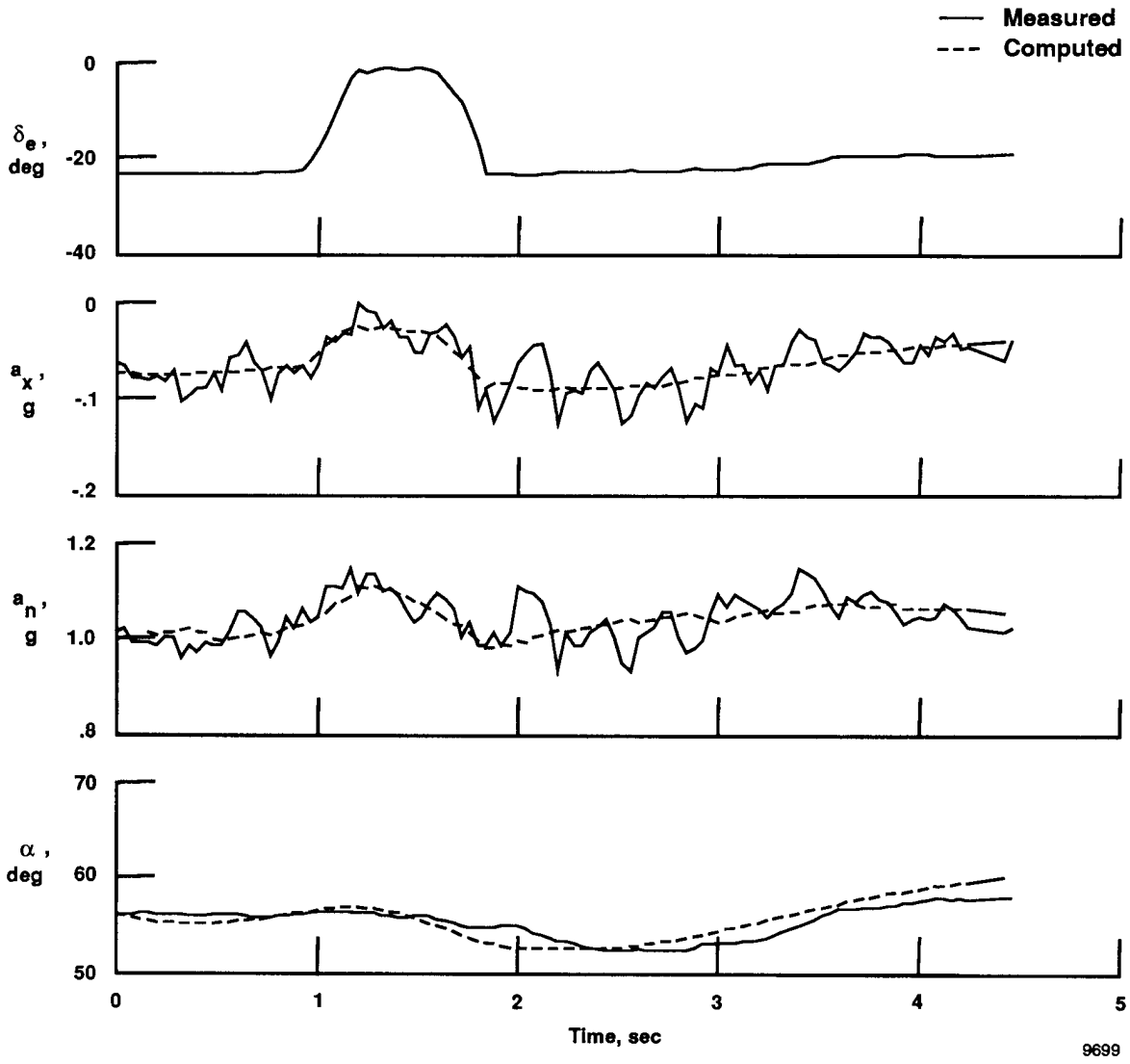

(a) Force axes.

Figure 12. Longitudinal maneuver at an average $\alpha = 55°$.

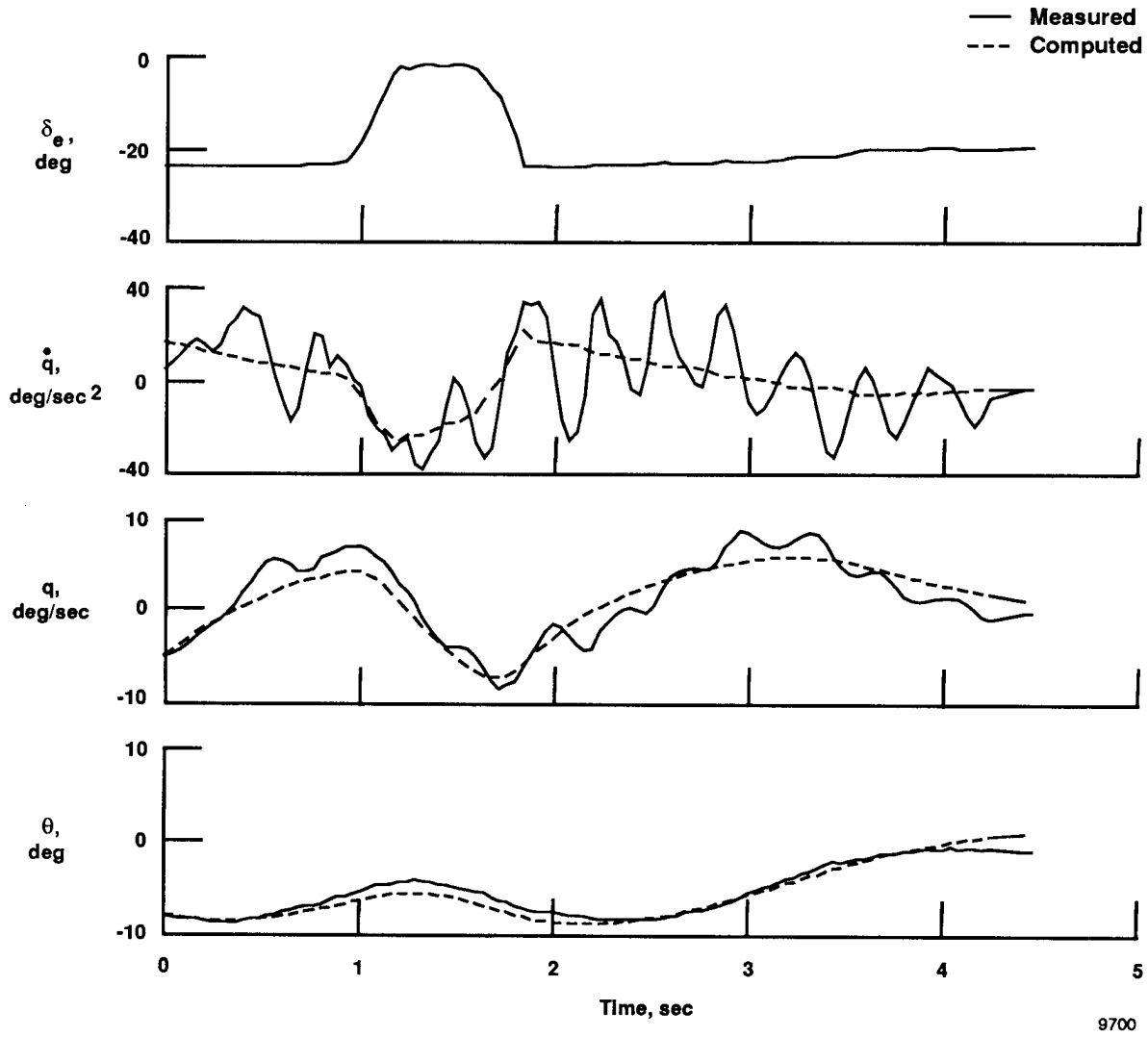

(b) Moment axis.

Figure 12. Concluded.

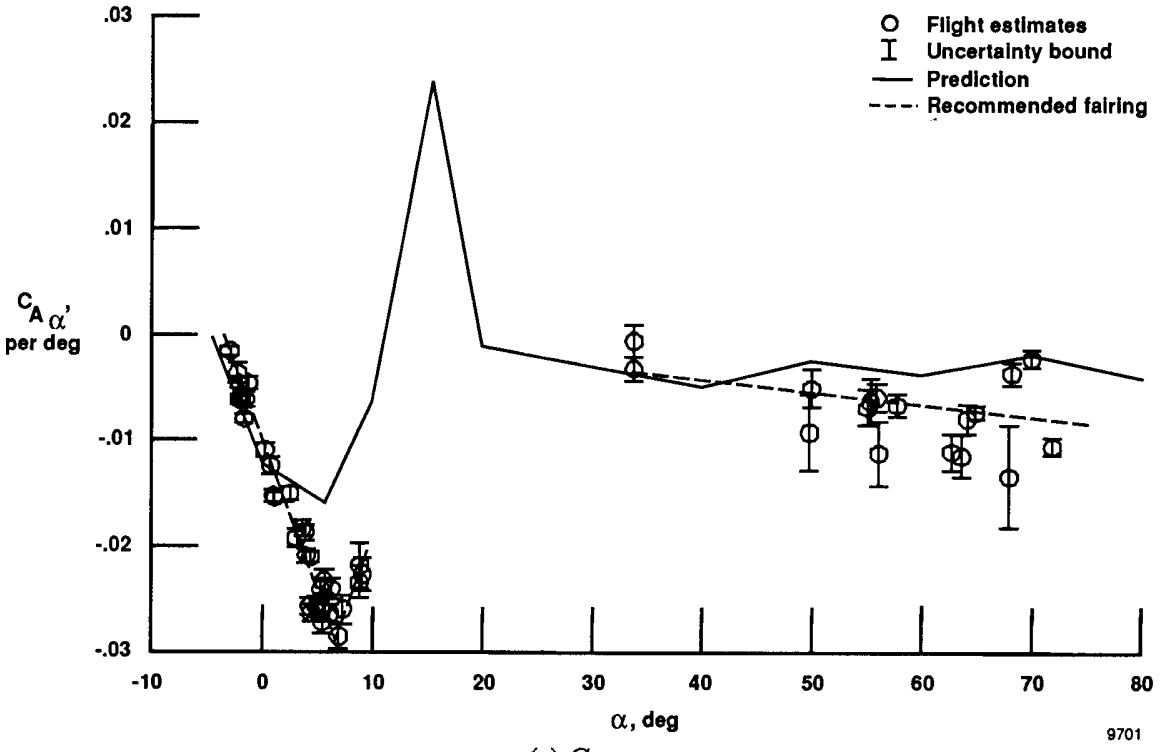

(a) C_{A_α}.

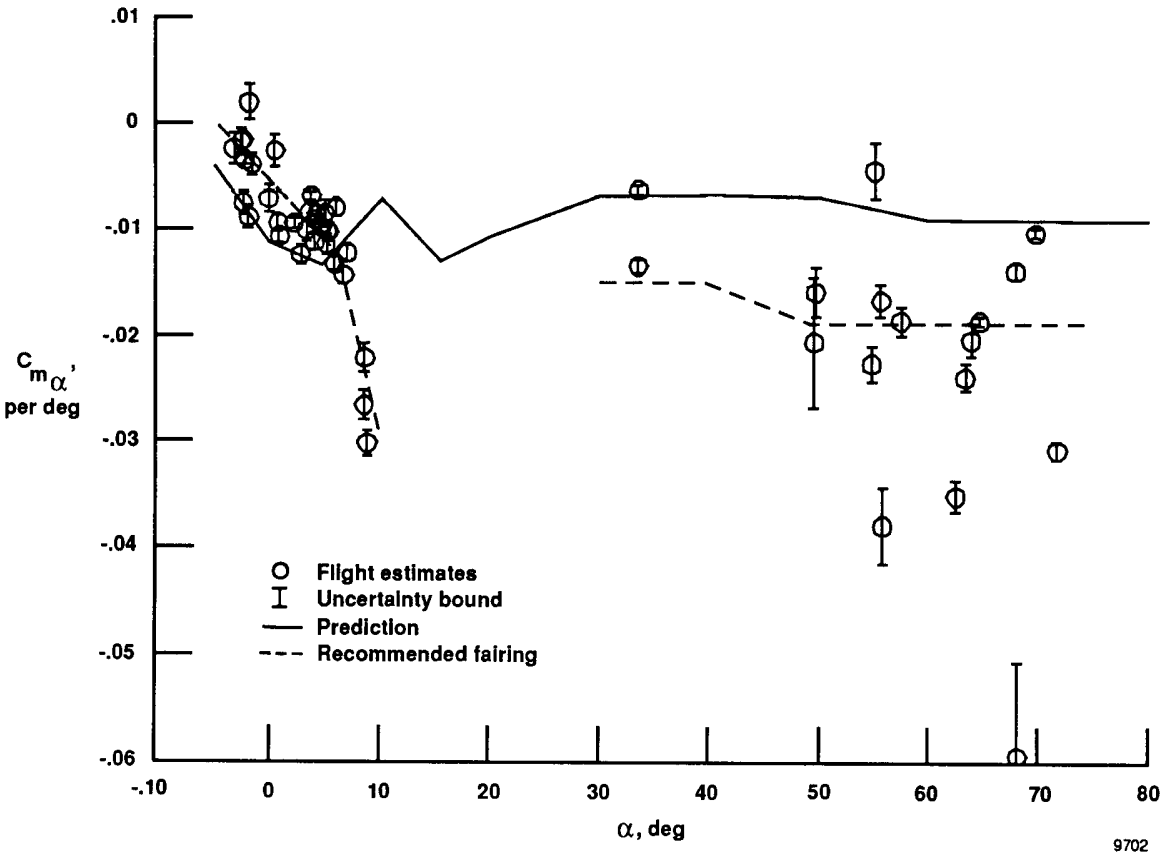

(b) C_{m_α}.

Figure 13.Longitudinal parameters.

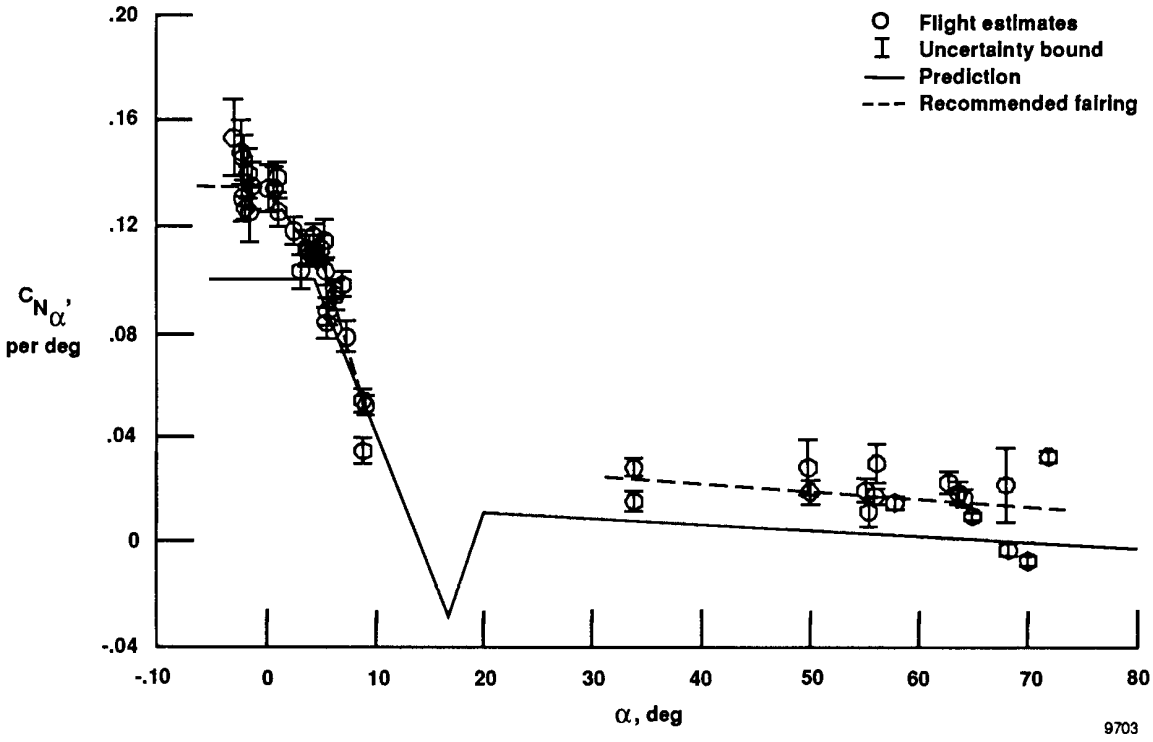

(c) C_{N_α}.

Figure 13. Continued.

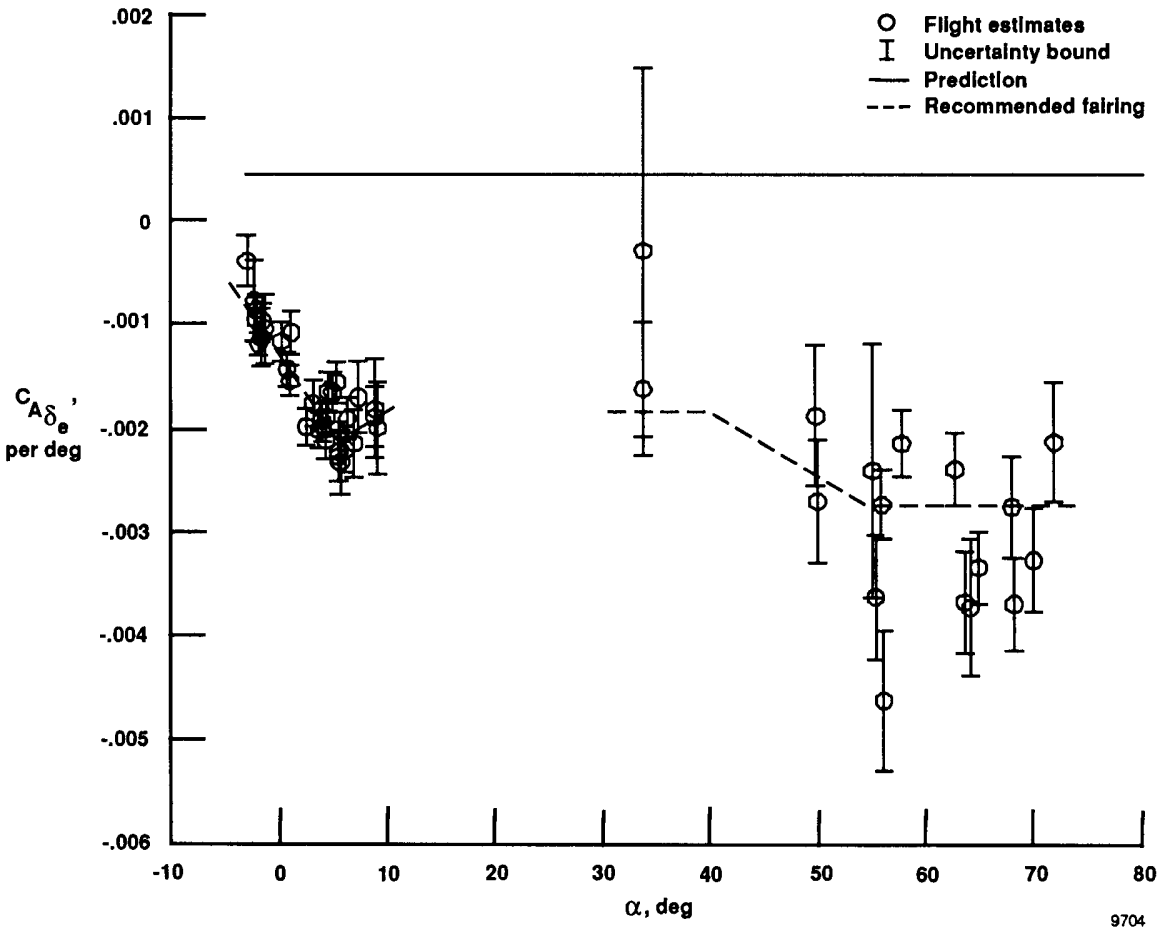

(d) $C_{A_{\delta_e}}$.

Figure 13. Continued.

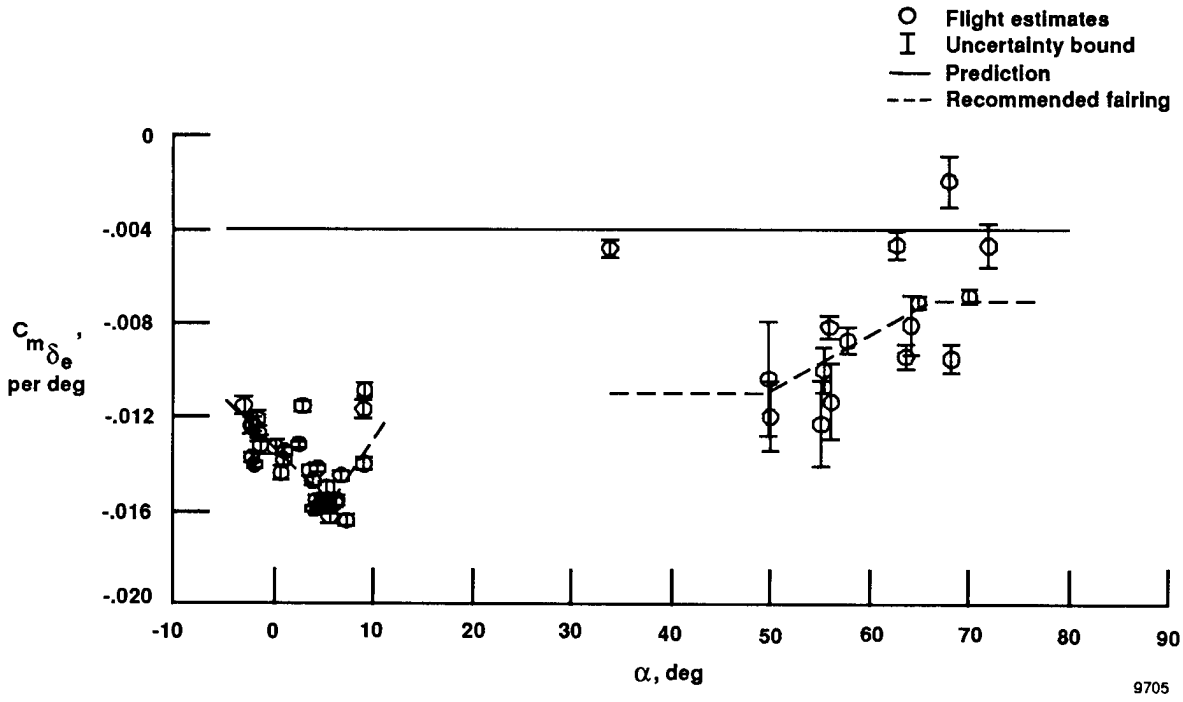

(e) $C_{m_{\delta_e}}$.

Figure 13. Continued.

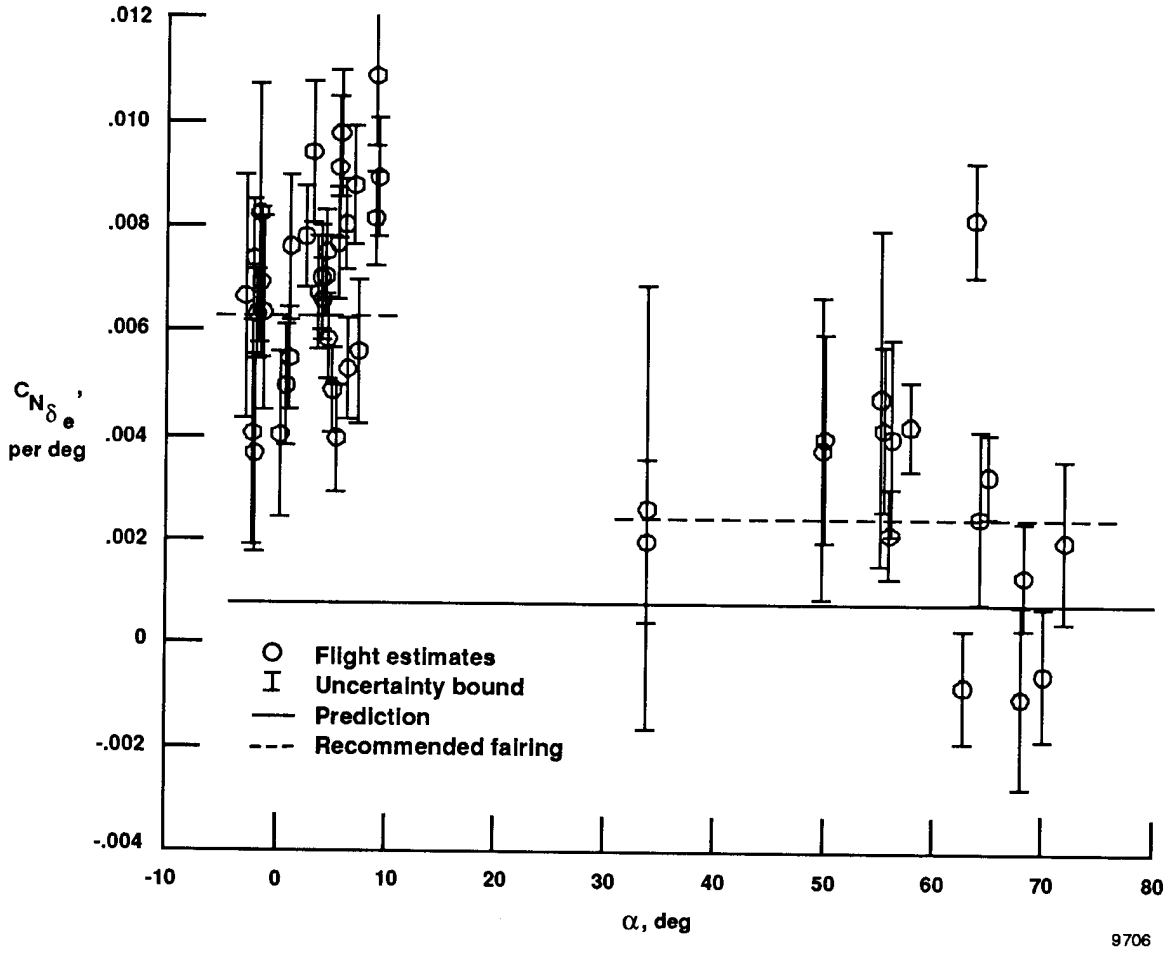

(f) $C_{N_{\delta_e}}$.

Figure 13. Continued.

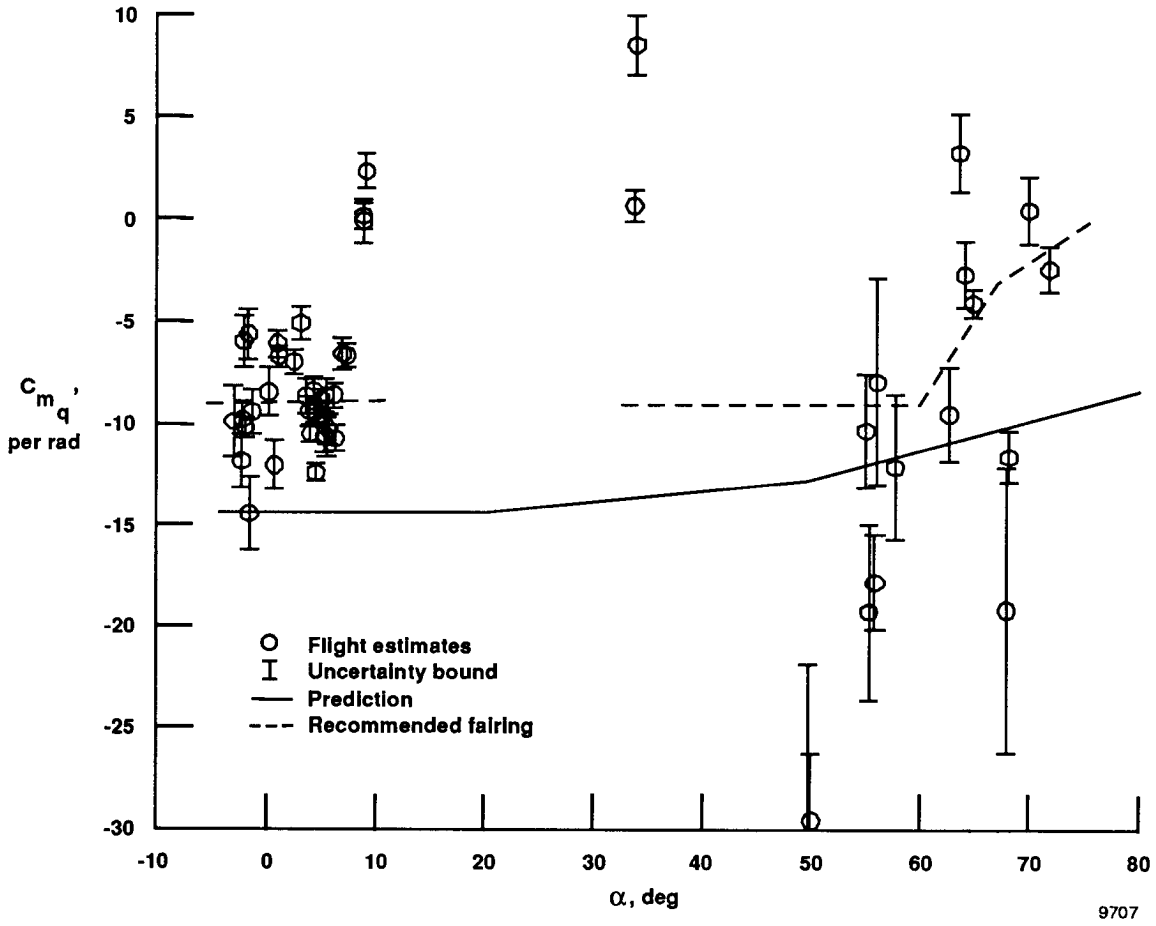

(g) C_{m_q}.

Figure 13. Concluded.

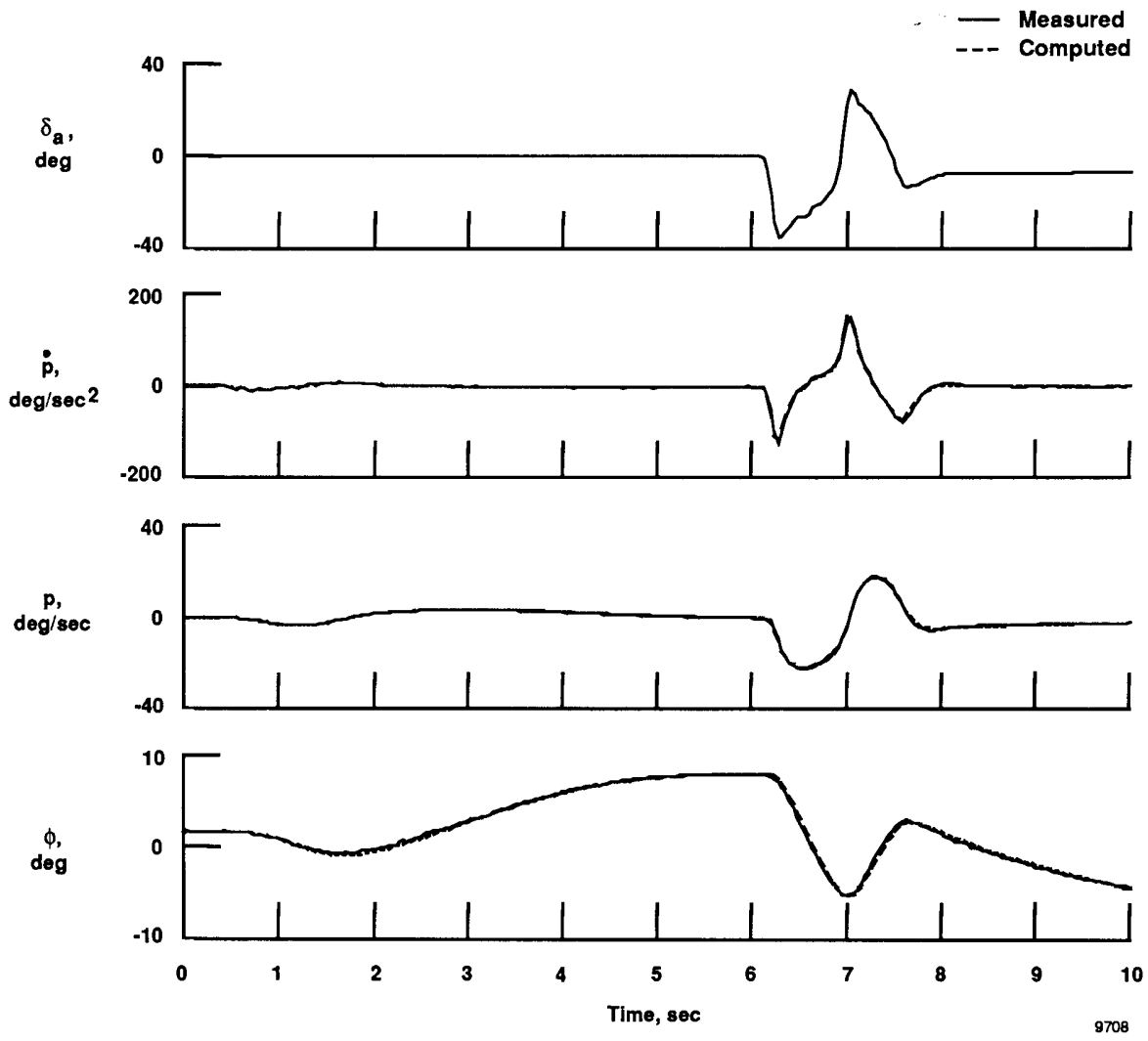

(a) Lateral axis.

Figure 14. Lateral-directional maneuver at an average $\alpha = 3.8°$.

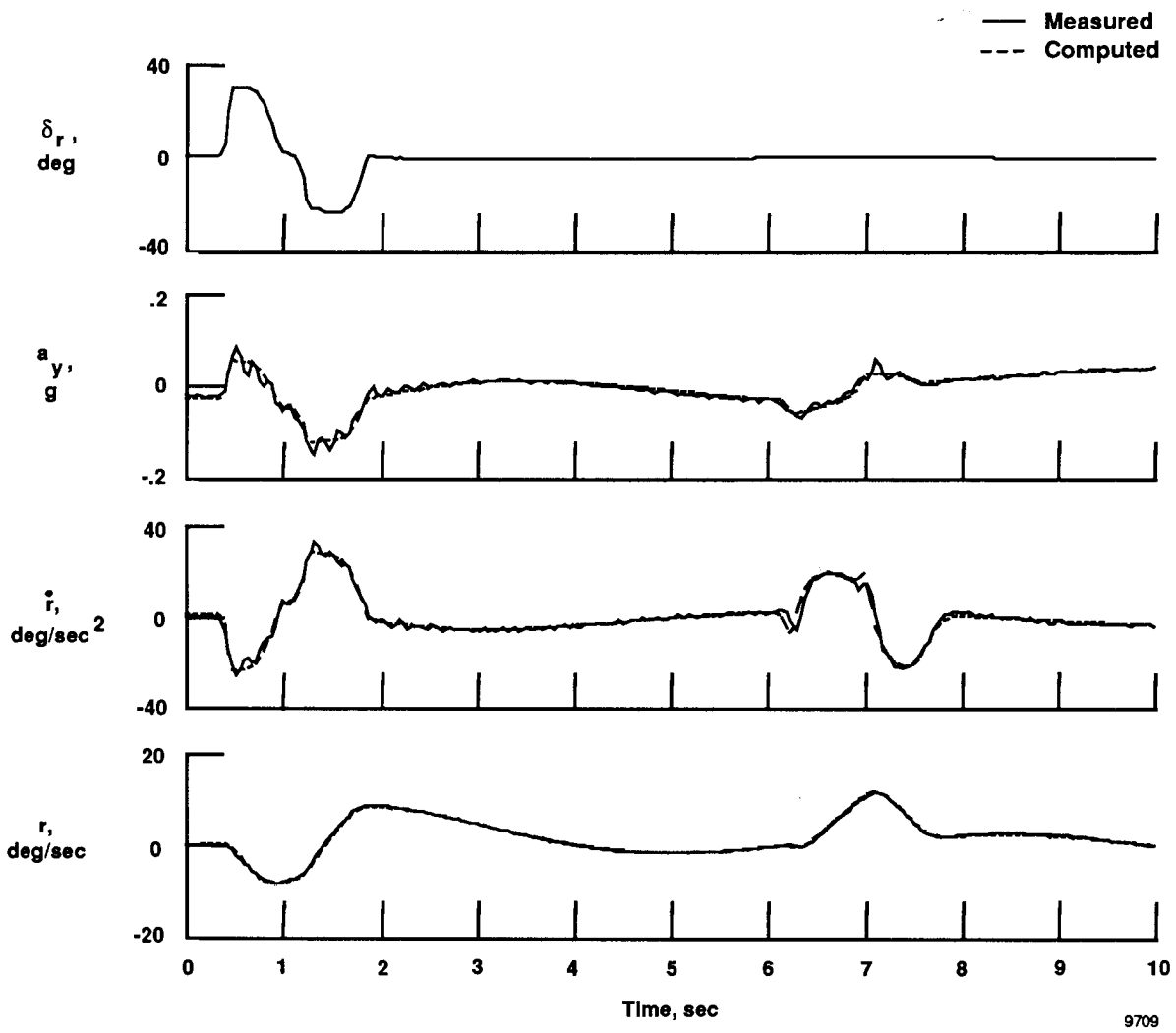

(b) Directional axis.

Figure 14. Concluded.

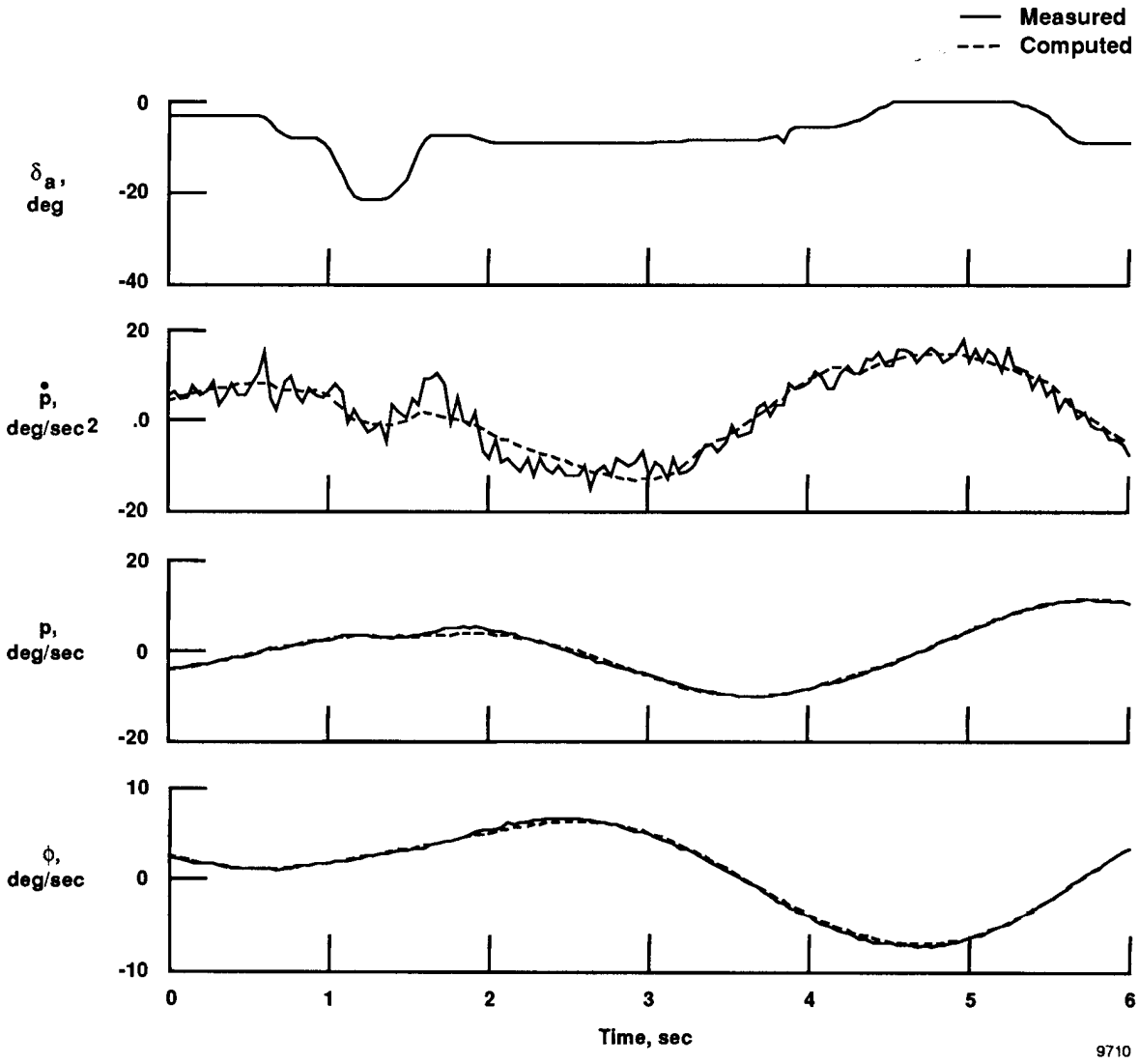

(a) Lateral axis.

Figure 15. Lateral-directional maneuver at an average $\alpha = 65°$.

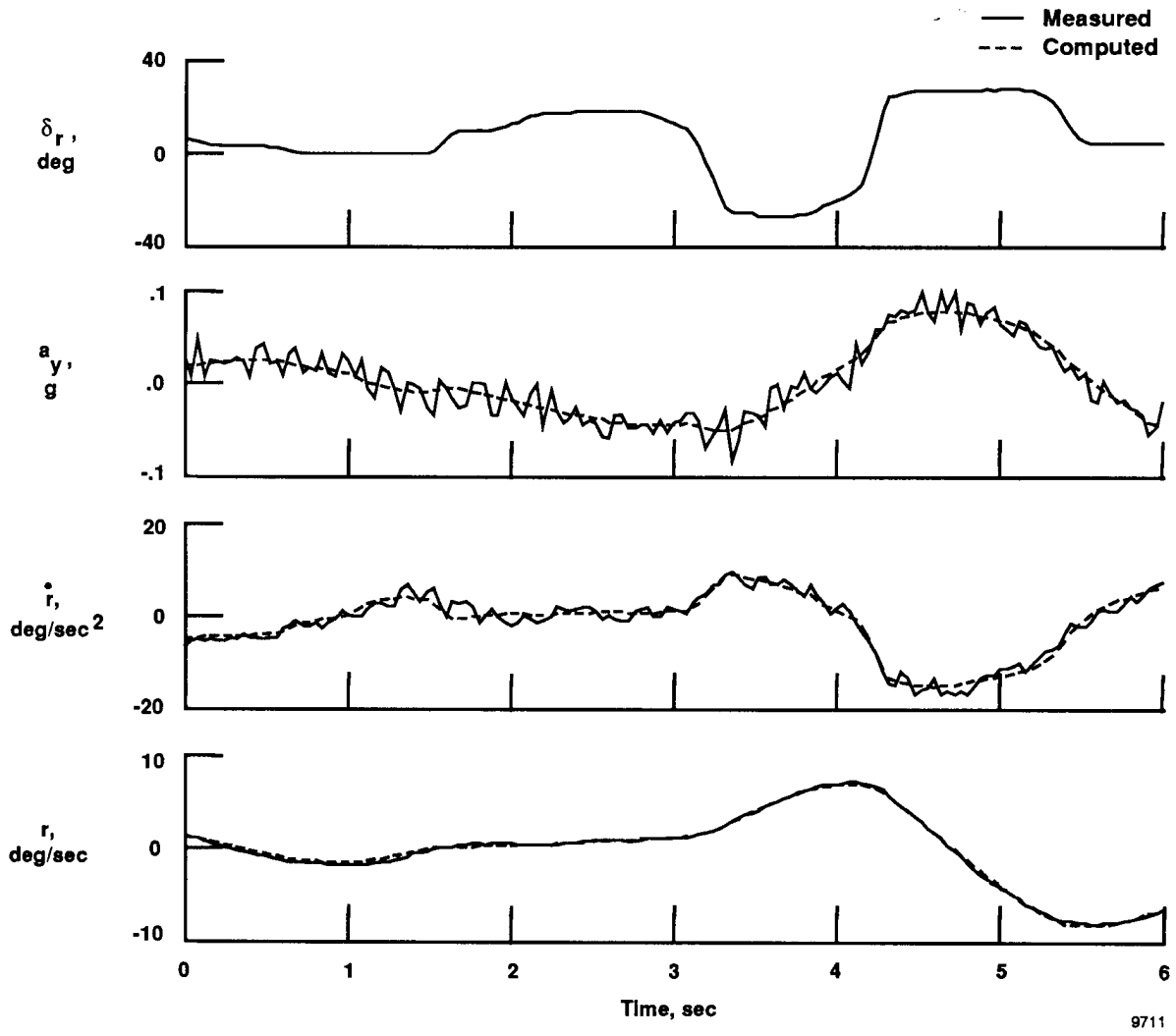

(b) Directional axis.
Figure 15. Concluded.

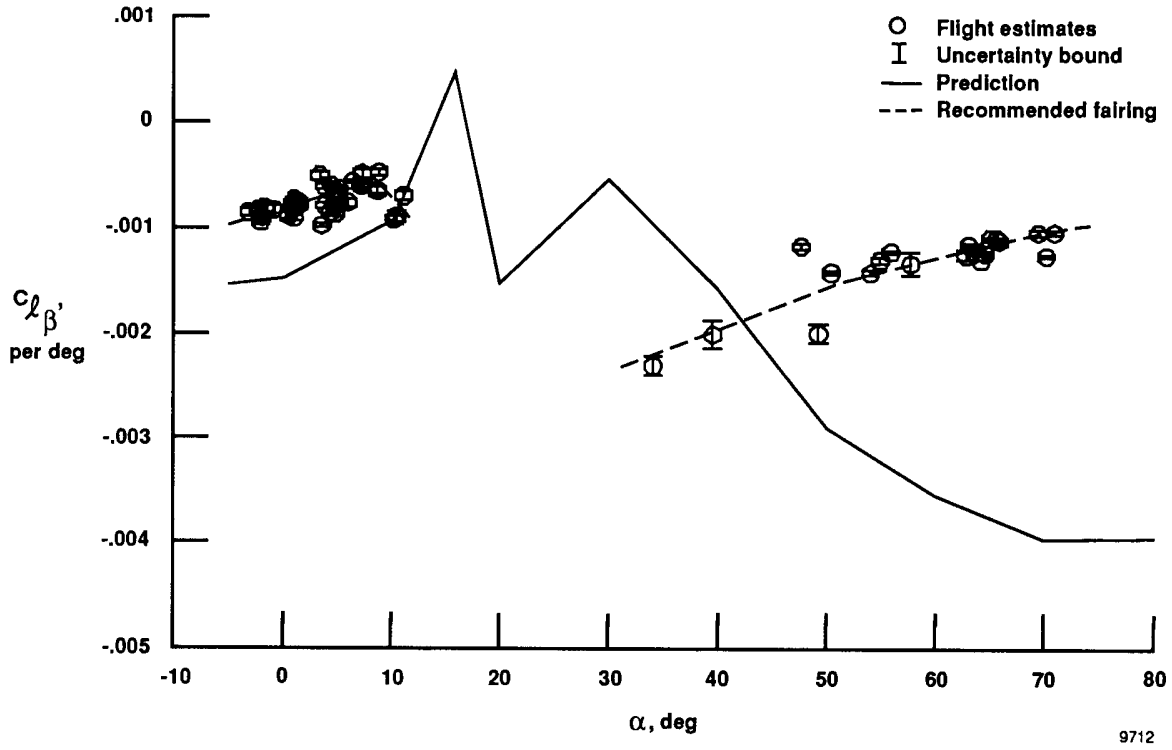

(a) C_{ℓ_β}.

Figure 16. Lateral-directional parameters.

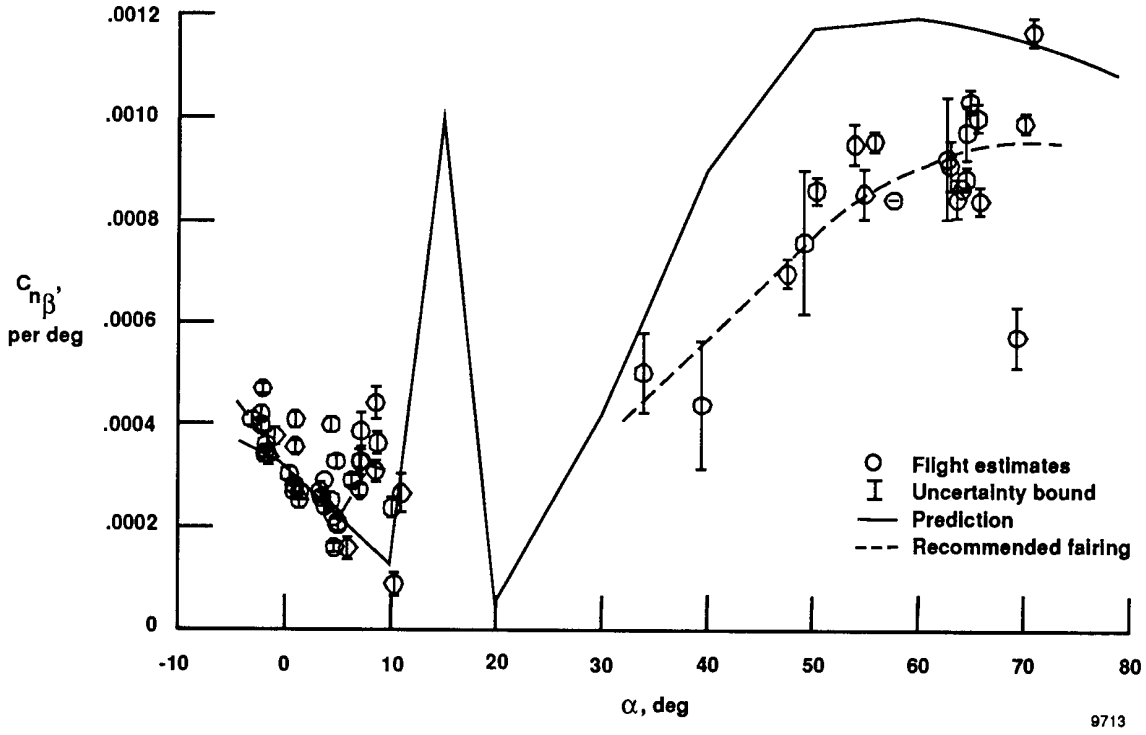

(b) C_{n_β}.

Figure 16. Continued.

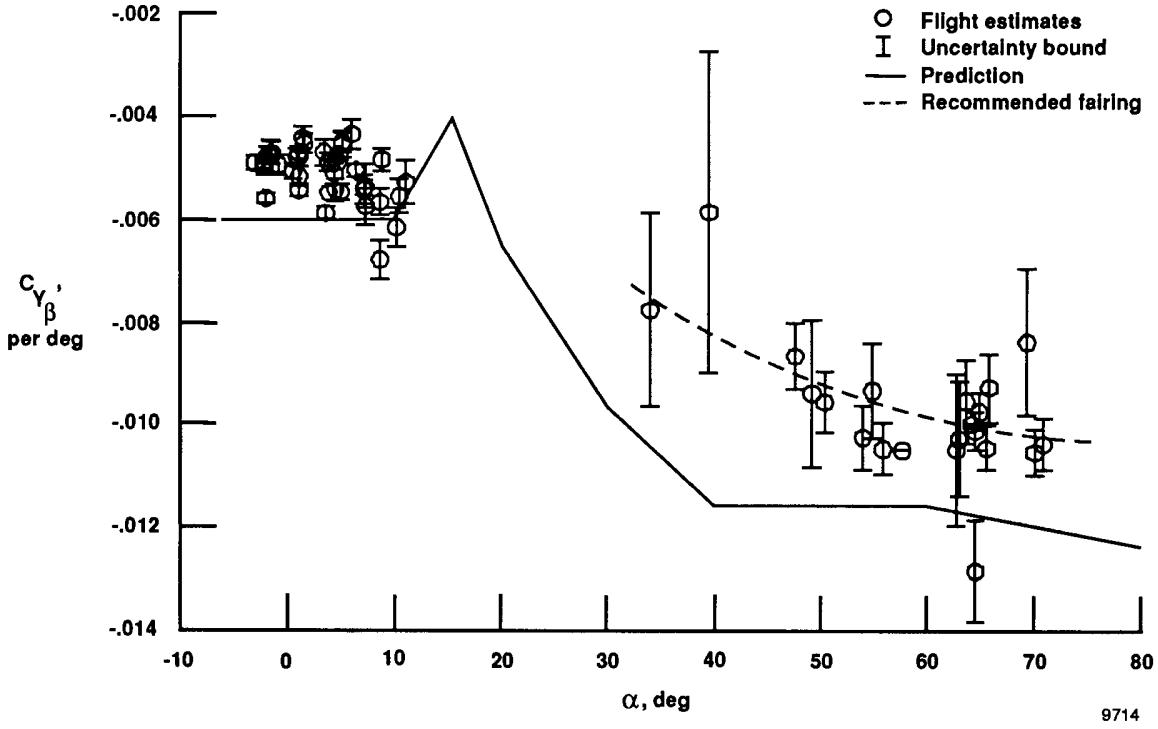

(c) C_{Y_β}.

Figure 16. Continued.

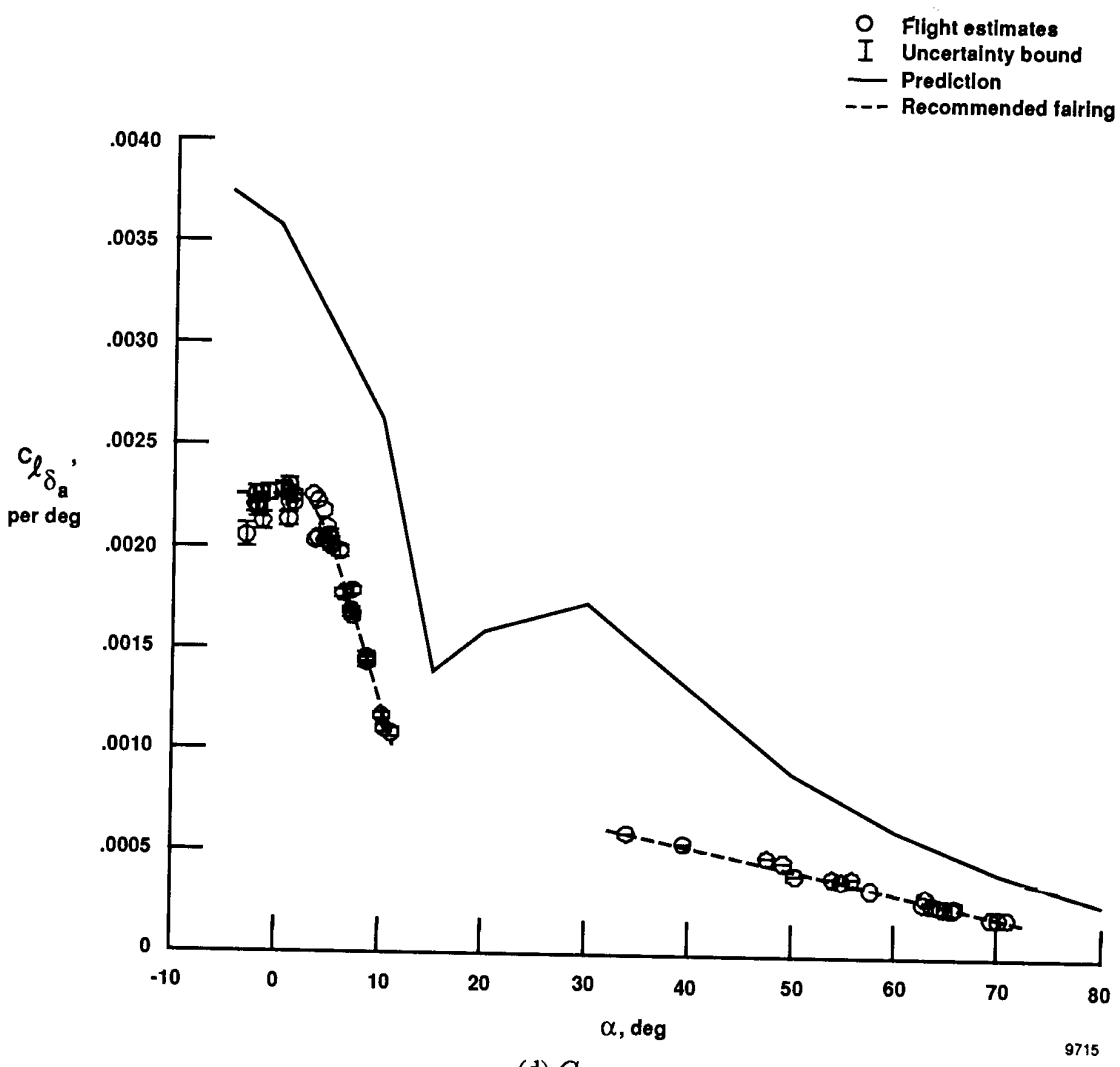

(d) $C_{\ell_{\delta_a}}$.

Figure 16. Continued.

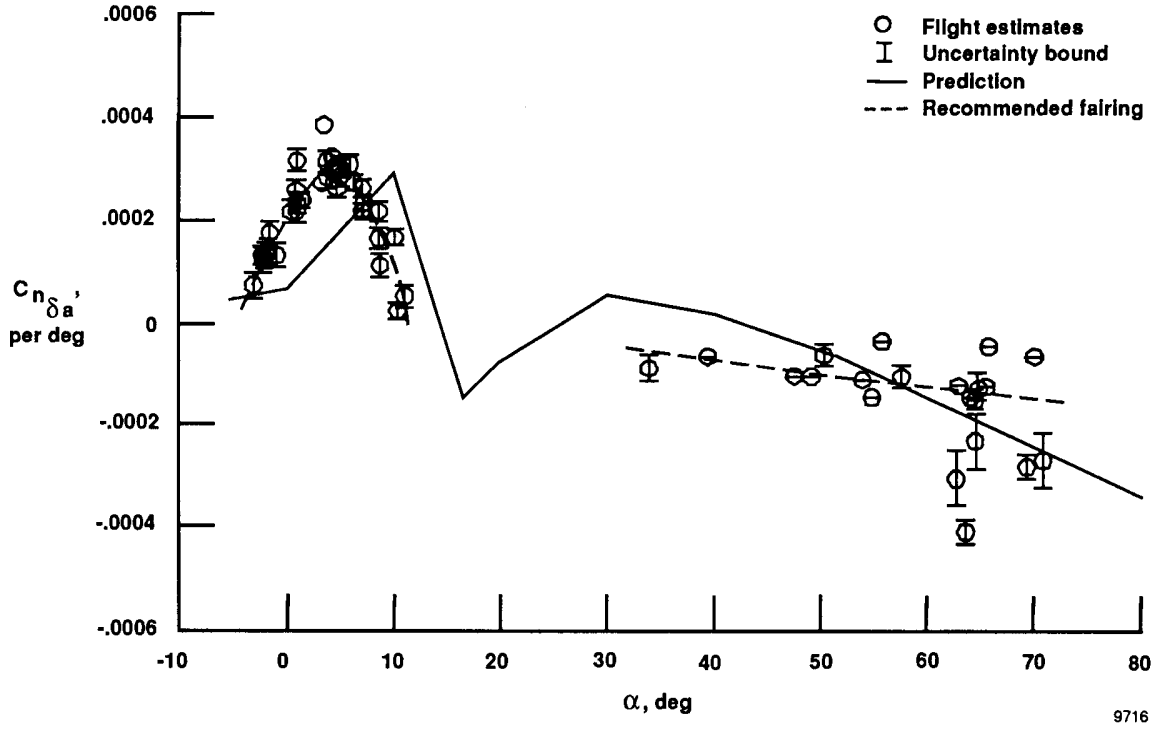

(e) $C_{n_{\delta_a}}$.

Figure 16. Continued.

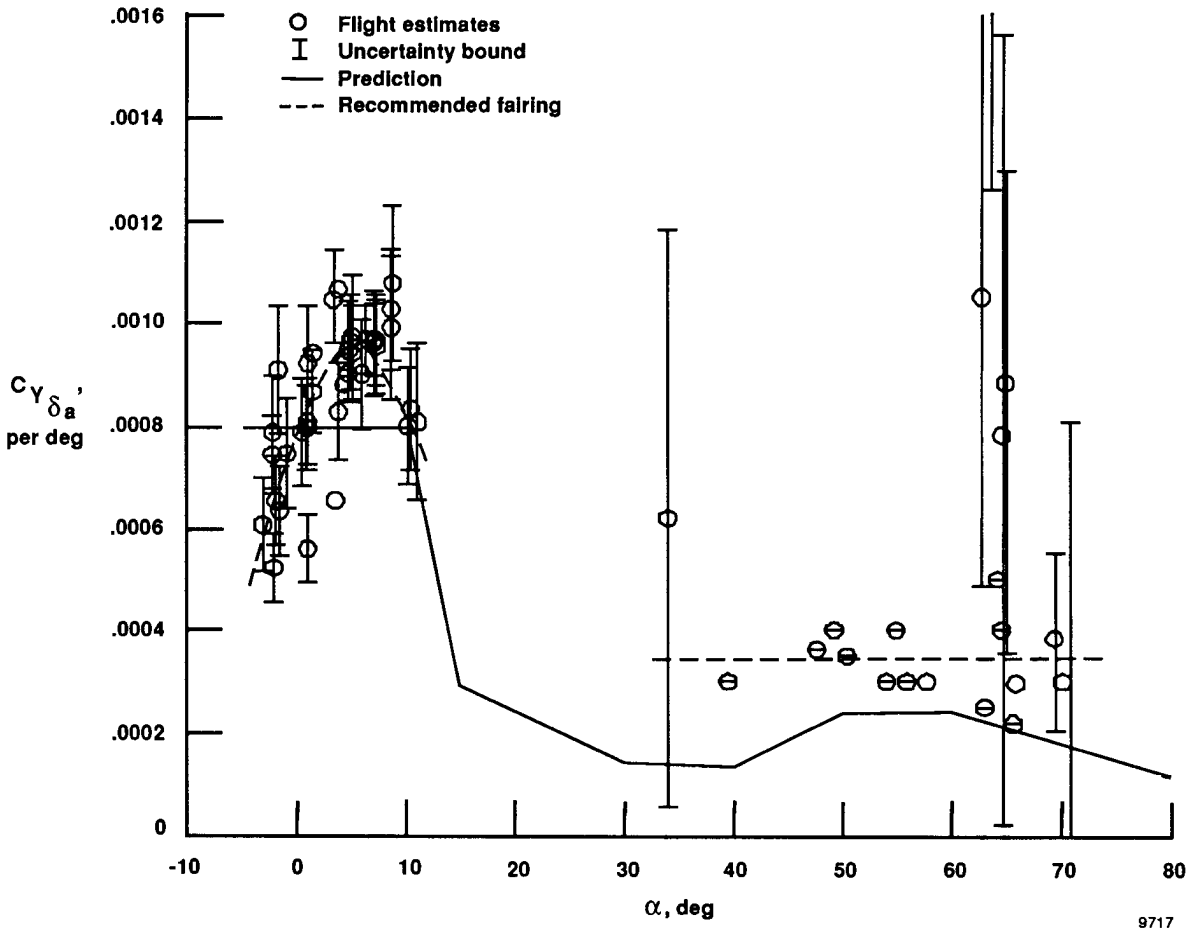

(f) $C_{Y_{\delta_a}}$.

Figure 16. Continued.

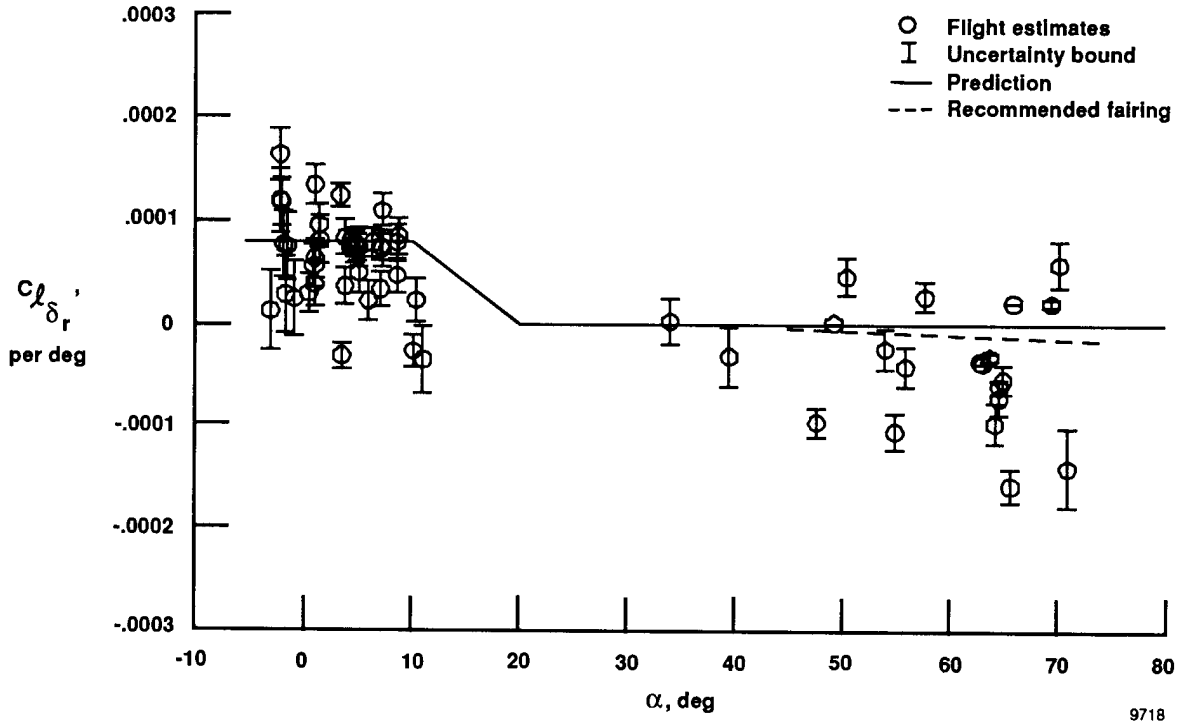

(g) $C_{\ell_{\delta_r}}$.

Figure 16. Continued.

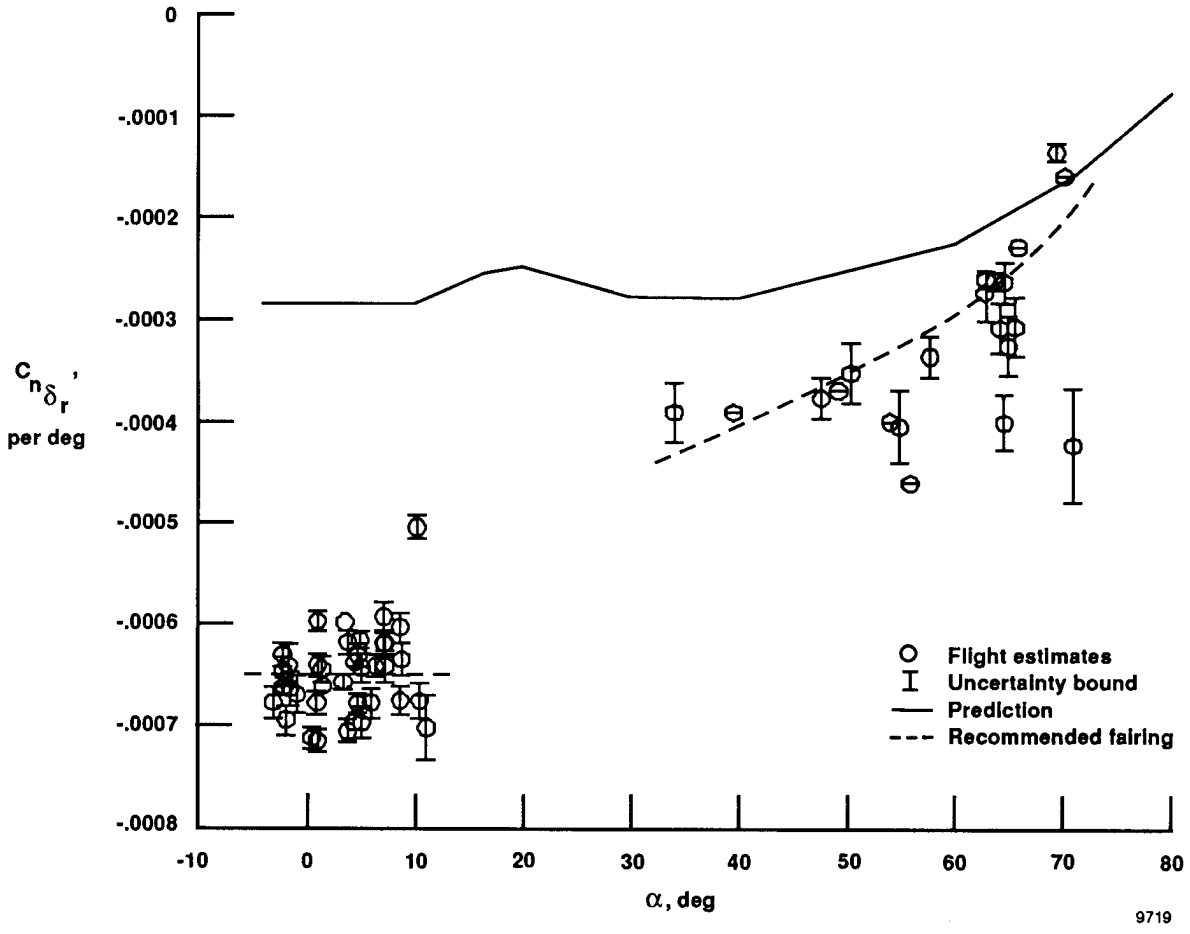

(h) $C_{n_{\delta_r}}$.

Figure 16. Continued.

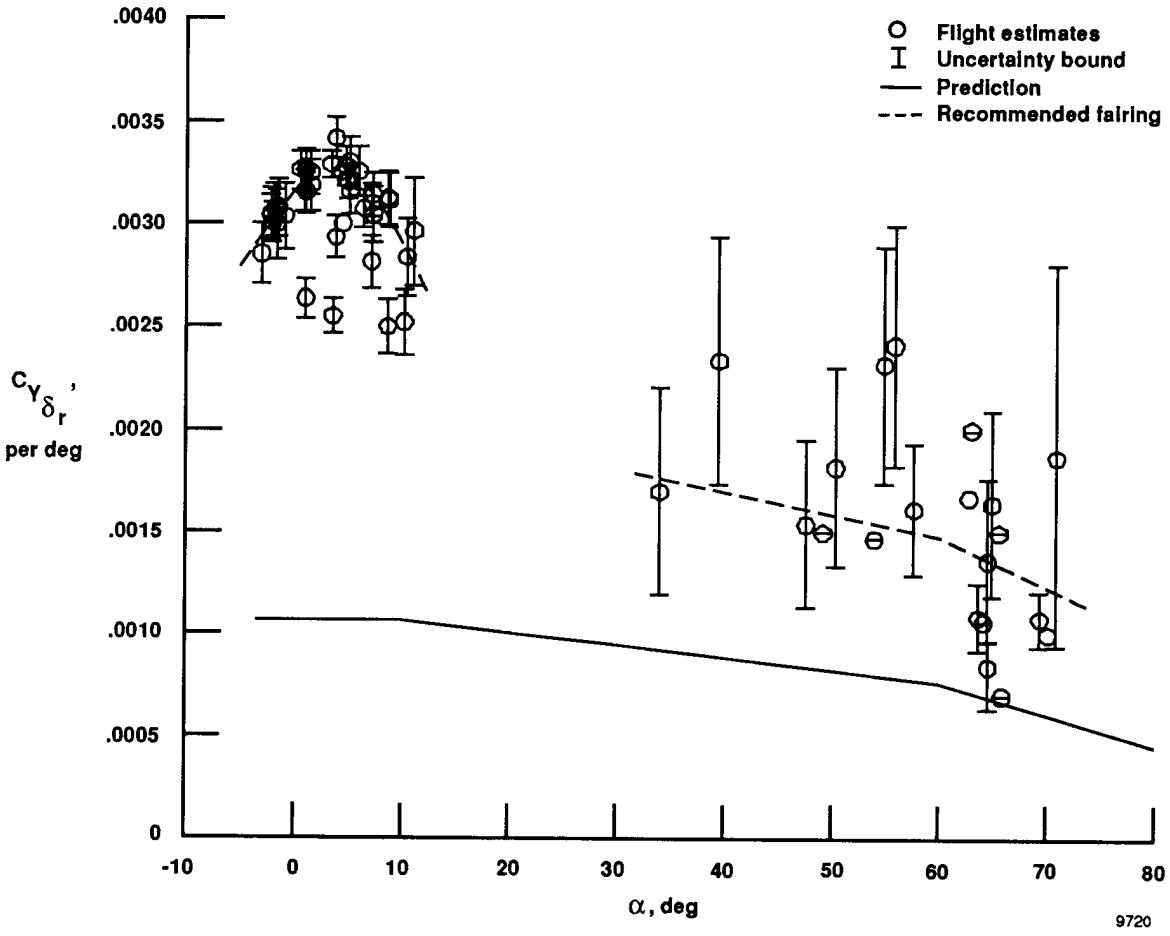

(i) $C_{Y_{\delta_r}}$.

Figure 16. Continued.

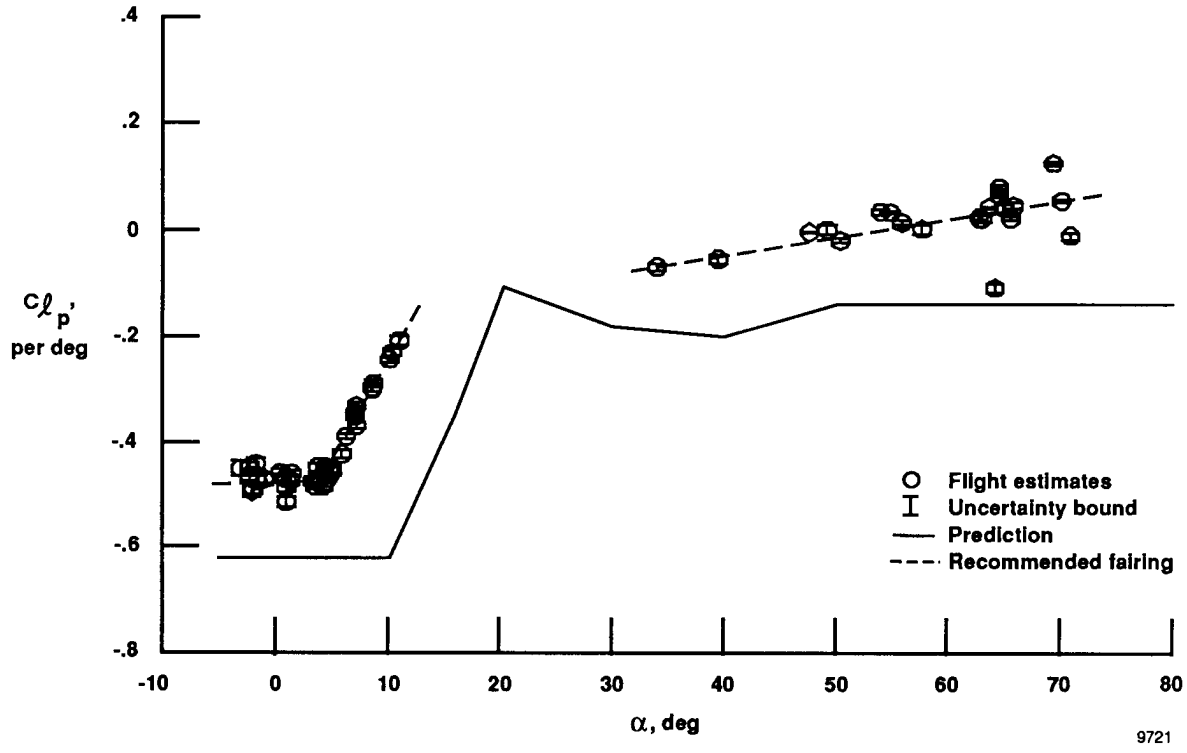

(j) C_{ℓ_p}.

Figure 16. Continued.

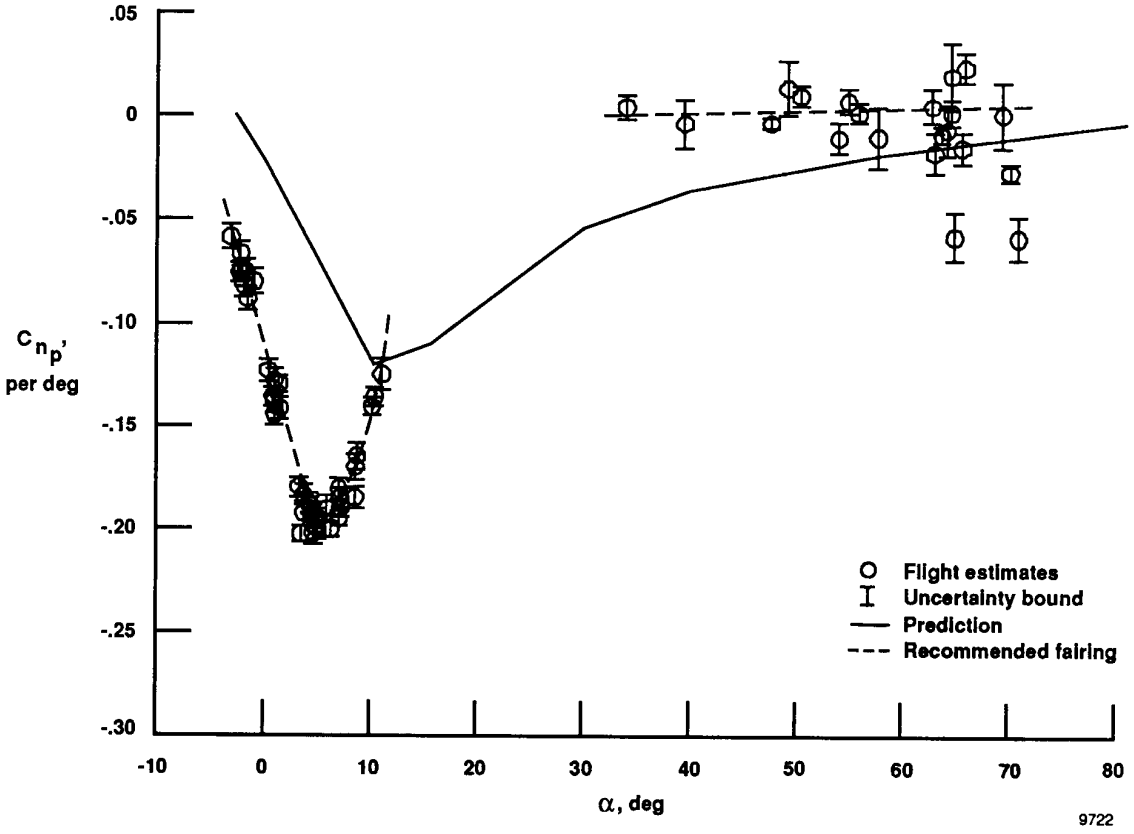

(k) C_{n_p}.

Figure 16. Continued.

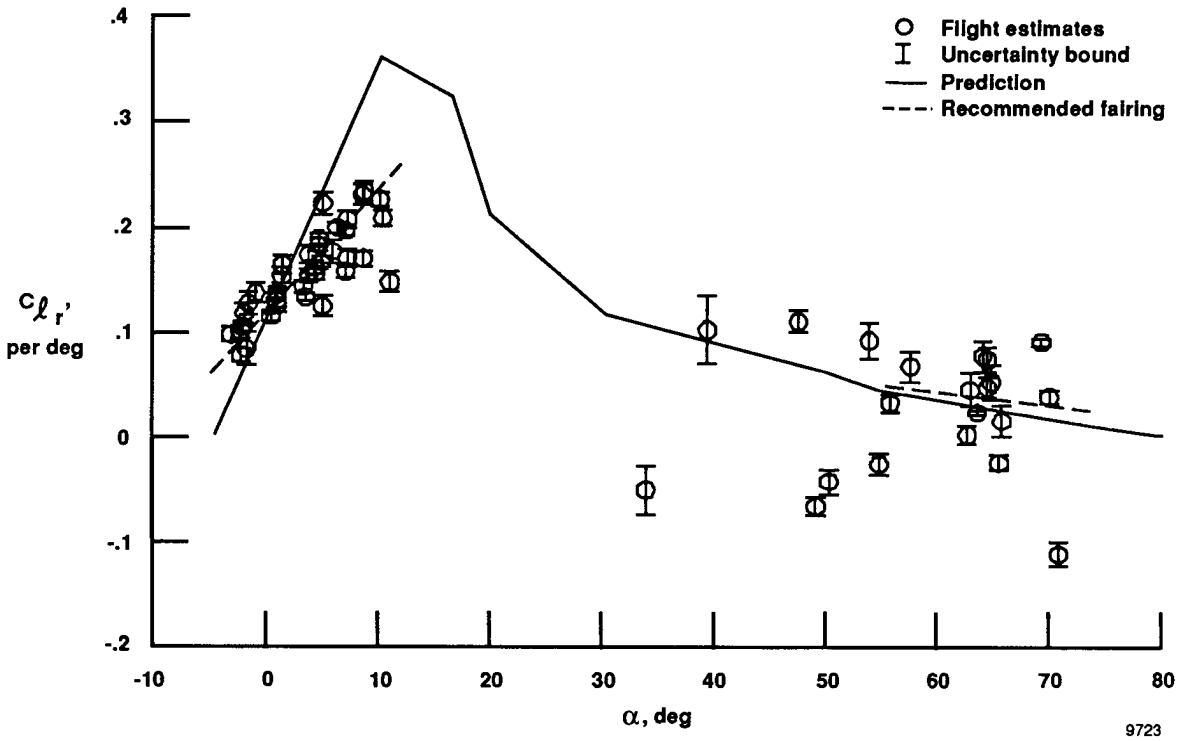

(l) C_{ℓ_r}.

Figure 16. Continued.

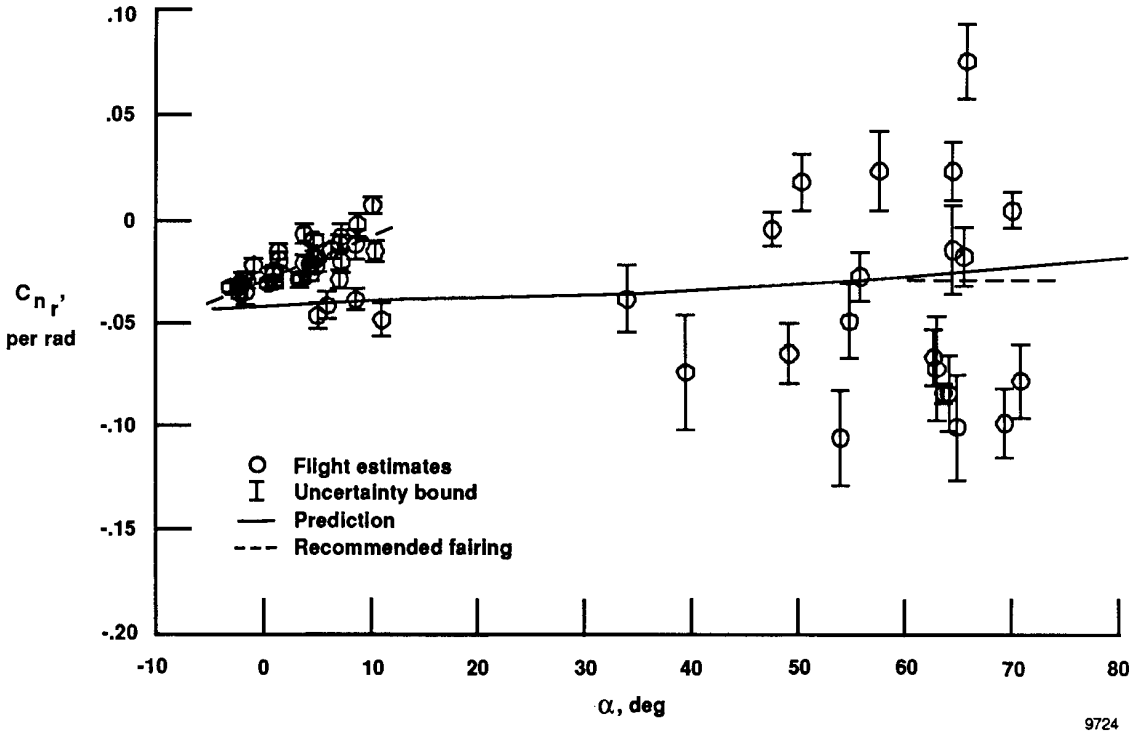

(m) C_{n_r}.

Figure 16. Concluded.

NASA
National Aeronautics and Space Administration

Report Documentation Page

1. Report No.	2. Government Accession No.	3. Recipient's Catalog No.
NASA TP-3022		

4. Title and Subtitle
Flight Characteristics of a Modified Schweizer SGS 1-36 Sailplane at Low and Very High Angles of Attack

5. Report Date
August 1990

6. Performing Organization Code

7. Author(s)
Alex G. Sim

8. Performing Organization Report No.
H-1563

10. Work Unit No.
RTOP 505-45-21

9. Performing Organization Name and Address
Ames Research Center
Dryden Flight Research Facility
P.O. Box 273, Edwards, CA 93523-0273

11. Contract or Grant No.

13. Type of Report and Period Covered
Technical Paper

12. Sponsoring Agency Name and Address
National Aeronautics and Space Administration
Washington, DC 20546-0001

14. Sponsoring Agency Code

15. Supplementary Notes

16. Abstract

A manned flight research program using a modified sailplane was conducted to very high angles of attack at the NASA Ames Research Center's Dryden Flight Research Facility. Piloting techniques were established that enabled the pilot to attain and stabilize on an angle of attack in the 30° to 72° range. Aerodynamic derivatives were estimated from the flight data for both low and very high angles of attack and are compared to wind-tunnel data. In addition, limited performance and trim data are presented.

17. Key Words (Suggested by Author(s))
Controlled deep stall; High-angle-of-attack flight; Parameter estimation; Parameter identification; Schweizer SGS 1-36 sailplane; Stability and control derivatives

18. Distribution Statement
Unclassified–Unlimited

Subject Category 08

19. Security Classif. (of this report)	20. Security Classif. (of this page)	21. No. of Pages	22. Price
Unclassified	Unclassified	48	A03

NASA FORM 1626 OCT 86

For sale by the National Technical Information Service, Springfield, VA 22161-2171.